Universität Hamburg

Synchrotron Research Institute

YEREVAN STATE UNIVERSITY

German-Armenian Joint Practical Course
on Accelerator Physics

Beam-Matter Interaction and Radiation Dose Measurements

Supervisor: Dr. Vitali Khachatryan

PIER
Partnership of
Universitat Hamburg and DESY

YEREVAN, ARMENIA
2025

Contents

1 Interactions of particles and radiation with matter

An online version of the book is published at doi.org/10.1017/9781009401531 .

Particles and radiation can be detected only through their interactions with matter. There are specific interactions for charged particles which are different from those of neutral particles, e.g. of photons. One can say that every interaction process can be used as a basis for a detector concept. The variety of these processes is quite rich and, as a consequence, a large number of detection devices for particles and radiation exist. In addition, for one and the same particle, different interaction processes at different energies may be relevant.

In this chapter, the main interaction mechanisms will be presented in a comprehensive fashion. Special effects will be dealt with when the individual detectors are being presented. The interaction processes and their cross sections will not be derived from basic principles but are presented only in their results, as they are used for particle detectors.

The main interactions of charged particles with matter are *ionisation* and *excitation*. For relativistic particles, *bremsstrahlung* energy losses must also be considered. Neutral particles must produce charged particles in an interaction that are then detected via their characteristic interaction processes. In the case of photons, these processes are the photoelectric effect, Compton scattering and pair production of electrons. The electrons produced in these *photon interactions* can be observed through their ionisation in the sensitive volume of the detector.

1.1 Interactions of charged particles

Charged particles passing through matter lose kinetic energy by *excitation* of bound electrons and by *ionisation*. Excitation processes like

$$\begin{aligned} e^- + \text{atom} &\rightarrow \text{atom}^* + e^- \\ &\hookrightarrow \text{atom} + \gamma \end{aligned} \tag{1.1}$$

lead to low-energy photons and are therefore useful for particle detectors which can record this luminescence. Of greater importance are pure scattering processes in which incident particles transfer a certain amount of their energy to atomic electrons so that they are liberated from the atom.

The *maximum transferable kinetic energy* to an electron depends on the mass m_0 and the momentum of the incident particle. Given the momentum of the incident particle

$$p = \gamma m_0 \beta c \ , \tag{1.2}$$

where γ is the Lorentz factor ($= E/m_0c^2$), $\beta c = v$ the velocity, and m_0 the rest mass, the maximum energy that may be transferred to an electron (mass m_e) is given by [1] (see also Problem 1.6)

$$E_{\text{kin}}^{\max} = \frac{2m_e c^2 \beta^2 \gamma^2}{1 + 2\gamma m_e/m_0 + (m_e/m_0)^2} = \frac{2m_e p^2}{m_0^2 + m_e^2 + 2m_e E/c^2} \ . \tag{1.3}$$

In this case, it makes sense to give the kinetic energy, rather than total energy, since the electron is already there and does not have to be produced. The kinetic energy E_{kin} is related to the total energy E according to

$$E_{\text{kin}} = E - m_0c^2 = c\sqrt{p^2 + m_0^2c^2} - m_0c^2 \ . \tag{1.4}$$

For low energies

$$2\gamma m_e/m_0 \ll 1 \tag{1.5}$$

and under the assumption that the incident particles are heavier than electrons ($m_0 > m_e$) Eq. (1.3) can be approximated by

$$E_{\text{kin}}^{\max} \approx 2m_e c^2 \beta^2 \gamma^2 \ . \tag{1.6}$$

A particle (e.g. a muon, $m_\mu c^2 = 106\,\text{MeV}$) with a Lorentz factor of $\gamma = E/m_0c^2 = 10$ corresponding to $E = 1.06\,\text{GeV}$ can transfer approximately $100\,\text{MeV}$ to an electron (mass $m_e c^2 = 0.511\,\text{MeV}$).

If one neglects the quadratic term in the denominator of Eq. (1.3), $(m_e/m_0)^2 \ll 1$, which is a good assumption for all incident particles except for electrons, it follows that

$$E_{\mathrm{kin}}^{\mathrm{max}} = \frac{p^2}{\gamma m_0 + m_0^2/2m_e} \ . \tag{1.7}$$

For relativistic particles $E_{\mathrm{kin}} \approx E$ and $pc \approx E$ holds. Consequently, the maximum transferable energy is

$$E^{\mathrm{max}} \approx \frac{E^2}{E + m_0^2 c^2/2m_e} \tag{1.8}$$

which for muons gives

$$E^{\mathrm{max}} = \frac{E^2}{E + 11\,\mathrm{GeV}} \ . \tag{1.9}$$

In the extreme relativistic case $\left(E \gg m_0^2 c^2/2m_e\right)$, the total energy can be transferred to the electron.

If the incident particle is an electron, these approximations are no longer valid. In this case, one gets, compare Eq. (1.3),

$$E_{\mathrm{kin}}^{\mathrm{max}} = \frac{p^2}{m_e + E/c^2} = \frac{E^2 - m_e^2 c^4}{E + m_e c^2} = E - m_e c^2 \ , \tag{1.10}$$

which is also expected in classical non-relativistic kinematics for particles of equal mass for a central collision.

1.1.1 Energy loss by ionisation and excitation

The treatment of the maximum transferable energy has already shown that incident electrons, in contrast to heavy particles ($m_0 \gg m_e$), play a special rôle. Therefore, to begin with, we give the energy loss for 'heavy' particles. Following Bethe and Bloch [2–8]*, the average energy loss $\mathrm{d}E$ per length $\mathrm{d}x$ is given by

$$-\frac{\mathrm{d}E}{\mathrm{d}x} = 4\pi N_{\mathrm{A}} r_e^2 m_e c^2 z^2 \frac{Z}{A} \frac{1}{\beta^2} \left(\ln \frac{2 m_e c^2 \gamma^2 \beta^2}{I} - \beta^2 - \frac{\delta}{2} \right) \ , \tag{1.11}$$

* For the following considerations and formulae, not only the original literature but also secondary literature was used, mainly [1, 4–12] and references therein.

where

z – charge of the incident particle in units of the elementary charge

Z, A – atomic number and atomic weight of the absorber

m_e – electron mass

r_e – classical electron radius ($r_e = \frac{1}{4\pi\varepsilon_0} \cdot \frac{e^2}{m_e c^2}$ with ε_0 – permittivity of free space)

N_A – Avogadro number (= number of atoms per gram atom) = $6.022 \cdot 10^{23}\,\mathrm{mol}^{-1}$

I – mean excitation energy, characteristic of the absorber material, which can be approximated by

$$I = 16\ Z^{0.9}\,\mathrm{eV} \quad \text{for } Z > 1\ .$$

To a certain extent, I also depends on the molecular state of the absorber atoms, e.g. $I = 15\,\mathrm{eV}$ for atomic and $19.2\,\mathrm{eV}$ for molecular hydrogen. For liquid hydrogen, I is $21.8\,\mathrm{eV}$.

δ – is a parameter which describes how much the extended transverse electric field of incident relativistic particles is screened by the charge density of the atomic electrons. In this way, the energy loss is reduced (*density effect*, 'Fermi plateau' of the energy loss). As already indicated by the name, this density effect is important in dense absorber materials. For gases under normal pressure and for not too high energies, it can be neglected.
For energetic particles, δ can be approximated by

$$\delta = 2\ln\gamma + \zeta\ ,$$

where ζ is a material-dependent constant.
Various approximations for δ and material dependences for parameters, which describe the density effect, are discussed extensively in the literature [9]. At very high energies

$$\delta/2 = \ln(\hbar\omega_\mathrm{p}/I) + \ln\beta\gamma - 1/2\ ,$$

where $\hbar\omega_\mathrm{p} = \sqrt{4\pi N_e r_e^3}\, m_e c^2/\alpha = 28.8\sqrt{\varrho\,\langle Z/A\rangle}\,\mathrm{eV}$ is the plasma energy (ϱ in $\mathrm{g/cm^3}$), N_e the electron density, and α the fine-structure constant.

A useful constant appearing in Eq. (1.11) is

$$4\pi N_{\mathrm{A}} r_e^2 m_e c^2 = 0.3071 \ \frac{\mathrm{MeV}}{\mathrm{g/cm^2}} \ . \tag{1.12}$$

In the logarithmic term of Eq. (1.11), the quantity $2m_e c^2 \gamma^2 \beta^2$ occurs in the numerator, which, according to Eq. (1.6), is identical to the maximum transferable energy. The average energy of electrons produced in the ionisation process in gases equals approximately the ionisation energy [2, 3].

If one uses the approximation for the maximum transferable energy, Eq. (1.6), and the shorthand

$$\kappa = 2\pi N_{\mathrm{A}} r_e^2 m_e c^2 z^2 \cdot \frac{Z}{A} \cdot \frac{1}{\beta^2} \ , \tag{1.13}$$

the *Bethe–Bloch formula* can be written as

$$-\frac{\mathrm{d}E}{\mathrm{d}x} = 2\kappa \left(\ln \frac{E_{\mathrm{kin}}^{\mathrm{max}}}{I} - \beta^2 - \frac{\delta}{2} \right) \ . \tag{1.14}$$

The energy loss $-\mathrm{d}E/\mathrm{d}x$ is usually given in units of $\mathrm{MeV/(g/cm^2)}$. The length unit $\mathrm{d}x$ (in $\mathrm{g/cm^2}$) is commonly used, because the energy loss per area density

$$\mathrm{d}x = \varrho \cdot \mathrm{d}s \tag{1.15}$$

with ϱ density (in $\mathrm{g/cm^3}$) and $\mathrm{d}s$ length (in cm) is largely independent of the properties of the material. This length unit $\mathrm{d}x$ consequently gives the area density of the material.

Equation (1.11) represents only an approximation for the energy loss of charged particles by ionisation and excitation in matter which is, however, precise at the level of a few per cent up to energies of several hundred GeV. However, Eq. (1.11) cannot be used for slow particles, i.e., for particles which move with velocities which are comparable to those of atomic electrons or slower. For these velocities ($\alpha z \gg \beta \geq 10^{-3}$, $\alpha = \frac{e^2}{4\pi\varepsilon_0 \hbar c}$: fine-structure constant) the energy loss is proportional to β. The energy loss of slow protons, e.g. in silicon, can be described by [10–12]

$$-\frac{\mathrm{d}E}{\mathrm{d}x} = 61.2 \ \beta \ \frac{\mathrm{GeV}}{\mathrm{g/cm^2}} \ , \quad \beta < 5 \cdot 10^{-3} \ . \tag{1.16}$$

Equation (1.11) is valid for all velocities

$$\beta \gg \alpha z \ . \tag{1.17}$$

Table 1.1. *Average energy loss of minimum-ionising particles in various materials [10–12]; gases for standard pressure and temperature*

Absorber	$\frac{\mathrm{d}E}{\mathrm{d}x}\big\vert_{\mathrm{min}}\,[\frac{\mathrm{MeV}}{\mathrm{g/cm^2}}]$	$\frac{\mathrm{d}E}{\mathrm{d}x}\big\vert_{\mathrm{min}}\,[\frac{\mathrm{MeV}}{\mathrm{cm}}]$
Hydrogen (H_2)	4.10	$0.37 \cdot 10^{-3}$
Helium	1.94	$0.35 \cdot 10^{-3}$
Lithium	1.64	0.87
Beryllium	1.59	2.94
Carbon (Graphite)	1.75	3.96
Nitrogen	1.82	$2.28 \cdot 10^{-3}$
Oxygen	1.80	$2.57 \cdot 10^{-3}$
Air	1.82	$2.35 \cdot 10^{-3}$
Carbon dioxide	1.82	$3.60 \cdot 10^{-3}$
Neon	1.73	$1.56 \cdot 10^{-3}$
Aluminium	1.62	4.37
Silicon	1.66	3.87
Argon	1.52	$2.71 \cdot 10^{-3}$
Titanium	1.48	6.72
Iron	1.45	11.41
Copper	1.40	12.54
Germanium	1.37	7.29
Tin	1.26	9.21
Xenon	1.25	$7.32 \cdot 10^{-3}$
Tungsten	1.15	22.20
Platinum	1.13	24.24
Lead	1.13	12.83
Uranium	1.09	20.66
Water	1.99	1.99
Lucite	1.95	2.30
Shielding concrete	1.70	4.25
Quartz (SiO_2)	1.70	3.74

Given this condition, the energy loss decreases like $1/\beta^2$ in the low-energy domain and reaches a broad minimum of ionisation near $\beta\gamma \approx 4$. Relativistic particles ($\beta \approx 1$), which have an energy loss corresponding to this minimum, are called *minimum-ionising particles* (MIPs). In light absorber materials, where the ratio $Z/A \approx 0.5$, the energy loss of minimum-ionising particles can be roughly represented by

$$-\left.\frac{\mathrm{d}E}{\mathrm{d}x}\right|_{\mathrm{min}} \approx 2\,\frac{\mathrm{MeV}}{\mathrm{g/cm^2}}\ . \tag{1.18}$$

In Table 1.1, the energy losses of minimum-ionising particles in different materials are given; for further values, see [10–12].

The energy loss increases again for $\gamma > 4$ (*logarithmic rise* or *relativistic rise*) because of the logarithmic term in the bracket of Eq. (1.11). The increase follows approximately a dependence like $2 \ln \gamma$.

The decrease of the energy loss at the ionisation minimum with increasing atomic number of the absorber originates mainly from the Z/A term in Eq. (1.11). A large fraction of the logarithmic rise relates to large energy transfers to few electrons in the medium (δ *rays* or knock-on electrons). Because of the density effect, the logarithmic rise of the energy loss saturates at high energies.

For heavy projectiles (e.g. like copper nuclei), the energy loss of slow particles is modified because, while being slowed down, electrons get attached to the incident nuclei, thereby decreasing their effective charge.

The energy loss by ionisation and excitation for muons in iron is shown in Fig. 1.1 [10, 11, 13].

The energy loss according to Eq. (1.11) describes only energy losses due to ionisation and excitation. At high energies, radiation losses become more and more important (see Sect. 1.1.5).

Figure 1.2 shows the ionisation energy loss for electrons, muons, pions, protons, deuterons and α particles in air [14].

Equation (1.11) gives only the average energy loss of charged particles by ionisation and excitation. For thin absorbers (in the sense of Eq. (1.15), average energy loss $\langle \Delta E \rangle \ll E_{\max}$), in particular, strong fluctuations around the average energy loss exist. The energy-loss distribution for thin absorbers is strongly asymmetric [2, 3].

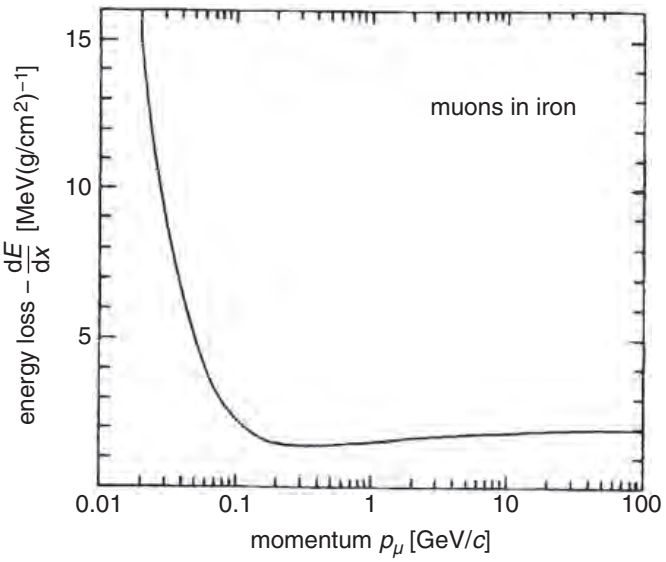

Fig. 1.1. Energy loss by ionisation and excitation for muons in iron and its dependence on the muon momentum.

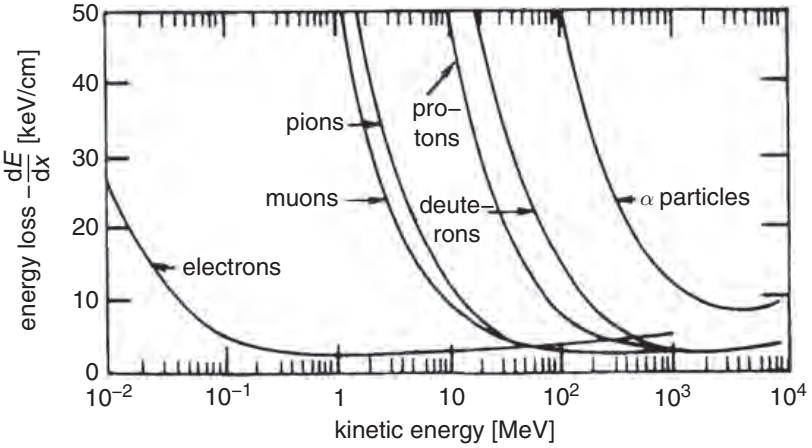

Fig. 1.2. Energy loss for electrons, muons, pions, protons, deuterons and α particles in air [14].

This behaviour can be parametrised by a *Landau distribution*. The Landau distribution is described by the inverse Laplace transform of the function s^s [15–18]. A reasonable approximation of the Landau distribution is given by [19–21]

$$L(\lambda) = \frac{1}{\sqrt{2\pi}} \cdot \exp\left[-\frac{1}{2}(\lambda + \mathrm{e}^{-\lambda})\right] \ , \tag{1.19}$$

where λ characterises the deviation from the *most probable energy loss*,

$$\lambda = \frac{\Delta E - \Delta E^{\mathrm{W}}}{\xi} \ , \tag{1.20}$$

ΔE – actual energy loss in a layer of thickness x,
ΔE^{W} – most probable energy loss in a layer of thickness x,

$$\xi = 2\pi N_{\mathrm{A}} r_e^2 m_e c^2 z^2 \frac{Z}{A} \cdot \frac{1}{\beta^2} \varrho x = \kappa \varrho x \tag{1.21}$$

(ϱ – density in g/cm^3, x – absorber thickness in cm).

The general formula for the most probable energy loss is [12]

$$\Delta E^{\mathrm{W}} = \xi \left[\ln\left(\frac{2m_e c^2 \gamma^2 \beta^2}{I}\right) + \ln\frac{\xi}{I} + 0.2 - \beta^2 - \delta(\beta\gamma)\right] \ . \tag{1.22}$$

For example, for argon and electrons of energies up to 3.54 MeV from a ^{106}Rh source the most probable energy loss is [19]

$$\Delta E^{\mathrm{W}} = \xi \left[\ln \left(\frac{2m_e c^2 \gamma^2 \beta^2}{I^2} \xi \right) - \beta^2 + 0.423 \right] \quad . \tag{1.23}$$

The most probable energy loss for minimum-ionising particles ($\beta\gamma = 4$) in 1 cm argon is $\Delta E^{\mathrm{W}} = 1.2$ keV, which is significantly smaller than the average energy loss of 2.71 keV [2, 3, 19, 22]. Figure 1.3 shows the energy-loss distribution of 3 GeV electrons in a thin-gap drift chamber filled with Ar/CH_4 (80:20) [23].

Experimentally, one finds that the actual energy-loss distribution is frequently broader than represented by the Landau distribution.

For thick absorber layers, the tail of the Landau distribution originating from high energy transfers, however, is reduced [24]. For very thick absorbers $\left(\frac{\mathrm{d}E}{\mathrm{d}x} \cdot x \gg 2m_e c^2 \beta^2 \gamma^2\right)$, the energy-loss distribution can be approximated by a Gaussian distribution.

The energy loss $\mathrm{d}E/\mathrm{d}x$ in a compound of various elements i is given by

$$\frac{\mathrm{d}E}{\mathrm{d}x} \approx \sum_i f_i \left. \frac{\mathrm{d}E}{\mathrm{d}x} \right|_i \quad , \tag{1.24}$$

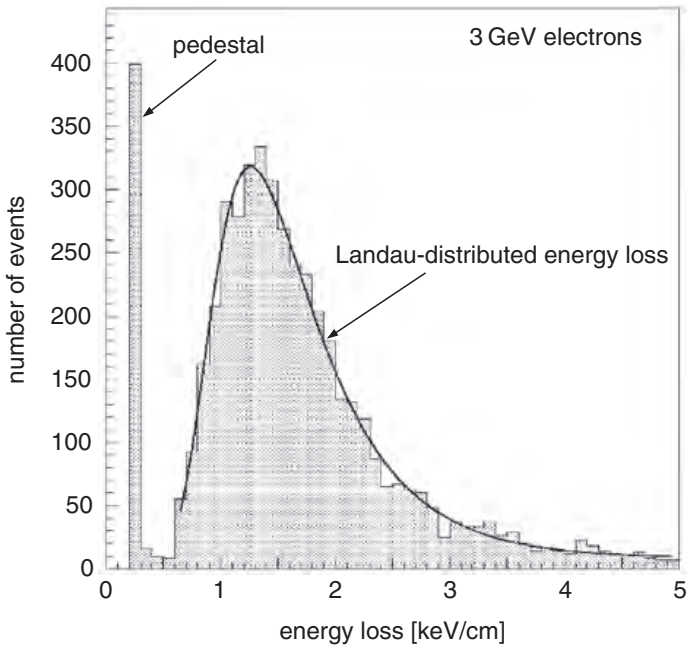

Fig. 1.3. Energy-loss distribution of 3 GeV electrons in a thin-gap drift chamber filled with Ar/CH_4 (80 : 20) [23].

where f_i is the mass fraction of the ith element and $\frac{\mathrm{d}E}{\mathrm{d}x}\big|_i$, the average energy loss in this element. Corrections to this relation because of the dependence of the ionisation constant on the molecular structure can be safely neglected.

The energy transfers to ionisation electrons can be so large that these electrons can cause further ionisation. These electrons are called δ rays or knock-on electrons. The energy spectrum of knock-on electrons is given by [1, 10–12, 25]

$$\frac{\mathrm{d}N}{\mathrm{d}E_{\mathrm{kin}}} = \xi \cdot \frac{F}{E_{\mathrm{kin}}^2} \tag{1.25}$$

for $I \ll E_{\mathrm{kin}} \leq E_{\mathrm{kin}}^{\mathrm{max}}$.

F is a spin-dependent factor of order unity, if $E_{\mathrm{kin}} \ll E_{\mathrm{kin}}^{\mathrm{max}}$ [12]. Of course, the energy spectrum of knock-on electrons falls to zero if the maximum transferable energy is reached. This kinematic limit also constrains the factor F [1, 25]. The spin dependence of the spectrum of the knock-on electrons only manifests itself close to the maximum transferable energy [1, 25].

The strong fluctuations of the energy loss in thin absorber layers are quite frequently not observed by a detector. Detectors only measure the energy which is actually deposited in their sensitive volume, and this energy may not be the same as the energy lost by the particle. For example, the energy which is transferred to knock-on electrons may only be partially deposited in the detector because the knock-on electrons can leave the sensitive volume of the detector.

Therefore, quite frequently it is of practical interest to consider only that part of the energy loss with energy transfers E smaller than a given cut value E_{cut}. This *truncated energy loss* is given by [10–12, 26]

$$-\frac{\mathrm{d}E}{\mathrm{d}x}\bigg|_{\leq E_{\mathrm{cut}}} = \kappa \left(\ln \frac{2m_e c^2 \beta^2 \gamma^2 E_{\mathrm{cut}}}{I^2} - \beta^2 - \delta \right) \ , \tag{1.26}$$

where κ is defined by Eq. (1.13). Equation (1.26) is similar, but not identical, to Eq. (1.11). Distributions of the truncated energy loss do not show a pronounced Landau tail as the distributions (1.19) for the mean value (1.11). Because of the density effect – expressed by δ in Eqs. (1.11) or (1.26), respectively – the truncated energy loss approaches a constant at high energies, which is given by the Fermi plateau.

So far, the energy loss by ionisation and excitation has been described for heavy particles. Electrons as incident particles, however, play a special rôle in the treatment of the energy loss. On the one hand, the total energy loss of electrons even at low energies (MeV range) is influenced by bremsstrahlung processes. On the other hand, the ionisation loss requires

special treatment because the mass of the incident particle and the target electron is the same.

In this case, one can no longer distinguish between the primary and secondary electron after the collision. Therefore, the energy-transfer probability must be interpreted in a different manner. One electron after the collision receives the energy E_{kin} and the other electron the energy $E - m_e c^2 - E_{\mathrm{kin}}$ (E is the total energy of the incident particle). All possible cases are considered if one allows the energy transfer to vary between 0 and $\frac{1}{2}(E - m_e c^2)$ and not up to $E - m_e c^2$.

This effect can be most clearly seen if in Eq. (1.11) the maximum energy transfer $E_{\mathrm{kin}}^{\mathrm{max}}$ of Eq. (1.6) is replaced by the corresponding expression for electrons. For relativistic particles, the term $\frac{1}{2}(E - m_e c^2)$ can be approximated by $E/2 = \frac{1}{2}\gamma m_e c^2$. Using $z = 1$, the ionisation loss of electrons then can be approximated by

$$-\frac{\mathrm{d}E}{\mathrm{d}x} = 4\pi N_{\mathrm{A}} r_e^2 m_e c^2 \frac{Z}{A} \cdot \frac{1}{\beta^2} \left(\ln \frac{\gamma m_e c^2}{2I} - \beta^2 - \frac{\delta^*}{2} \right) \quad , \tag{1.27}$$

where δ^* takes a somewhat different value for electrons compared to the parameter δ appearing in Eq. (1.11). A more precise calculation considering the specific differences between incident heavy particles and electrons yields a more exact formula for the energy loss of electrons due to ionisation and excitation [27],

$$\begin{aligned} -\frac{\mathrm{d}E}{\mathrm{d}x} = 4\pi N_{\mathrm{A}} r_e^2 m_e c^2 \frac{Z}{A} \cdot \frac{1}{\beta^2} \Bigg[& \ln \frac{\gamma m_e c^2 \beta \sqrt{\gamma - 1}}{\sqrt{2} I} \\ & + \frac{1}{2}(1 - \beta^2) - \frac{2\gamma - 1}{2\gamma^2} \ln 2 + \frac{1}{16} \left(\frac{\gamma - 1}{\gamma} \right)^2 \Bigg] \quad . \end{aligned} \tag{1.28}$$

This equation agrees with the general Bethe–Bloch relation (1.11) within 10%–20%. It takes into account the kinematics of electron–electron collisions and also screening effects.

The treatment of the ionisation loss of positrons is similar to that of electrons if one considers that these particles are of equal mass, but not identical charge.

For completeness, we also give the ionisation loss of positrons [28]:

$$\begin{aligned} -\frac{\mathrm{d}E}{\mathrm{d}x} = 4\pi N_{\mathrm{A}} r_e^2 m_e c^2 \frac{Z}{A} \frac{1}{\beta^2} \Bigg\{ & \ln \frac{\gamma m_e c^2 \beta \sqrt{\gamma - 1}}{\sqrt{2} I} \\ & - \frac{\beta^2}{24} \left[23 + \frac{14}{\gamma + 1} + \frac{10}{(\gamma + 1)^2} + \frac{4}{(\gamma + 1)^3} \right] \Bigg\} \quad . \end{aligned} \tag{1.29}$$

Since positrons are antiparticles of electrons, there is, however, an additional consideration: if positrons come to rest, they will annihilate with

an electron normally into two photons which are emitted anticollinearly. Both photons have energies of 511 keV in the centre-of-mass system, corresponding to the rest mass of the electrons. The *cross section for annihilation* in flight is given by [28]

$$\sigma(Z,E) = \frac{Z\pi r_e^2}{\gamma+1}\left[\frac{\gamma^2+4\gamma+1}{\gamma^2-1}\ln(\gamma+\sqrt{\gamma^2-1}) - \frac{\gamma+3}{\sqrt{\gamma^2-1}}\right] \quad . \tag{1.30}$$

More details about the ionisation process of elementary particles, in particular, its spin dependence, can be taken from the books of Rossi and Sitar *et al.* [1–3].

1.1.2 Channelling

The energy loss of charged particles as described by the Bethe–Bloch formula needs to be modified for crystals where the collision partners are arranged on a regular lattice. By looking into a crystal it becomes immediately clear that the energy loss along certain crystal directions will be quite different from that along a non-aligned direction or in an amorphous substance. The motion along such channelling directions is governed mainly by coherent scattering on strings and planes of atoms rather than by the individual scattering off single atoms. This leads to anomalous energy losses of charged particles in crystalline materials [29].

It is obvious from the crystal structure that charged particles can only be channelled along a crystal direction if they are moving more or less parallel to crystal axes. The critical angle necessary for *channelling* is small (approx. 0.3° for $\beta \approx 0.1$) and decreases with energy. For the axial direction ($\langle 111 \rangle$, body diagonal) it can be estimated by

$$\psi\,[\text{degrees}] = 0.307 \cdot [z \cdot Z/(E \cdot d)]^{0.5} \quad , \tag{1.31}$$

where z and Z are the charges of the incident particle and the crystal atom, E is the particle's energy in MeV, and d is the interatomic spacing in Å. ψ is measured in degrees [30].

For protons ($z = 1$) passing through a silicon crystal ($Z = 14; d = 2.35\,\text{Å}$), the critical angle for channelling along the direction-of-body diagonals becomes

$$\psi = 13\,\mu\text{rad}/\sqrt{E\,[\text{TeV}]} \quad . \tag{1.32}$$

For planar channelling along the face diagonals ($\langle 110 \rangle$ axis) in silicon one gets [29]

$$\psi = 5\,\mu\text{rad}/\sqrt{E\,[\text{TeV}]} \quad . \tag{1.33}$$

Of course, the channelling process also depends on the charge of the incident particle.

For a field inside a crystal of silicon atoms along the ⟨110⟩ crystal direction, one obtains a value of $1.3 \cdot 10^{10}\,\mathrm{V/cm}$. This field extends over macroscopic distances and can be used for the deflection of high-energy charged particles using bent crystals [30].

Channelled positive particles are kept away from a string of atoms and consequently suffer a relatively small energy loss. Figure 1.4 shows the energy-loss spectra for $15\,\mathrm{GeV}/c$ protons passing through a $740\,\mu\mathrm{m}$ thick germanium crystal [30]. The energy loss of channelled protons is lower by about a factor of 2 compared to random directions through the crystal.

1.1.3 Ionisation yield

The average energy loss by ionisation and excitation can be transformed into a number of electron–ion pairs produced along the track of a charged particle. One must distinguish between *primary ionisation*, that is the number of primarily produced electron–ion pairs, and the *total ionisation*. A sufficiently large amount of energy can be transferred to some primarily produced electrons so that they also can ionise (knock-on electrons). This secondary ionisation together with the primary ionisation forms the total ionisation.

The average energy required to form an electron–ion pair (W value) exceeds the ionisation potential of the gas because, among others, inner shells of the gas atoms can also be involved in the ionisation process,

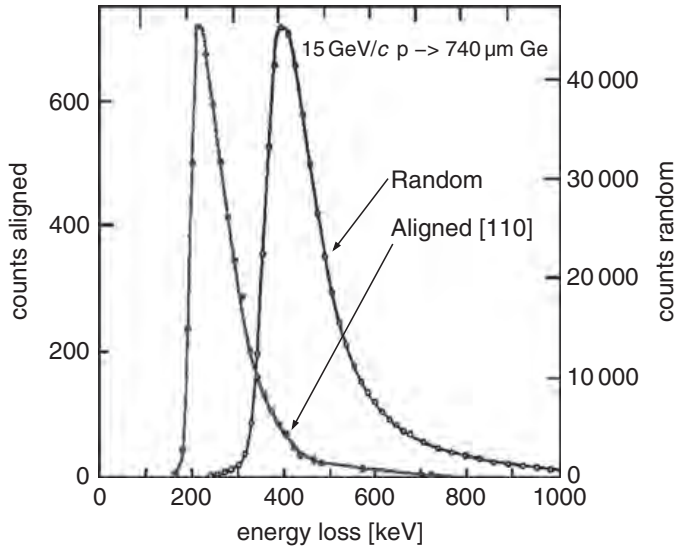

Fig. 1.4. The energy-loss spectra for $15\,\mathrm{GeV}/c$ protons passing through a $740\,\mu\mathrm{m}$ thick germanium crystal [30].

Table 1.2. *Compilation of some properties of gases. Given is the average effective ionisation potential per electron I_0, the average energy loss W per produced ion pair, the number of primary (n_p), and total (n_T) produced electron–ion pairs per cm at standard pressure and temperature for minimum-ionising particles [10, 11, 31–33]*

Gas	Density ϱ [g/cm^3]	I_0 [eV]	W [eV]	n_p [cm^{-1}]	n_T [cm^{-1}]
H_2	$8.99 \cdot 10^{-5}$	15.4	37	5.2	9.2
He	$1.78 \cdot 10^{-4}$	24.6	41	5.9	7.8
N_2	$1.25 \cdot 10^{-3}$	15.5	35	10	56
O_2	$1.43 \cdot 10^{-3}$	12.2	31	22	73
Ne	$9.00 \cdot 10^{-4}$	21.6	36	12	39
Ar	$1.78 \cdot 10^{-3}$	15.8	26	29	94
Kr	$3.74 \cdot 10^{-3}$	14.0	24	22	192
Xe	$5.89 \cdot 10^{-3}$	12.1	22	44	307
CO_2	$1.98 \cdot 10^{-3}$	13.7	33	34	91
CH_4	$7.17 \cdot 10^{-4}$	13.1	28	16	53
C_4H_{10}	$2.67 \cdot 10^{-3}$	10.8	23	46	195

and a fraction of the energy of the incident particle can be dissipated by excitation processes which do not lead to free electrons. The W value of a material is constant for relativistic particles and increases only slightly for low velocities of incident particles.

For gases, the W values are around 30 eV. They can, however, strongly depend on impurities in the gas. Table 1.2 shows the W values for some gases together with the number of primary (n_p) and total (n_T) electron–ion pairs produced by minimum-ionising particles (see Table 1.1) [10, 11, 31–33].

The numerical values for n_p are somewhat uncertain because experimentally it is very difficult to distinguish between primary and secondary ionisation. The total ionisation (n_T) can be computed from the total energy loss ΔE in the detector according to

$$n_\mathrm{T} = \frac{\Delta E}{W} \ . \tag{1.34}$$

This is only true if the transferred energy is completely deposited in the sensitive volume of the detector.

In solid-state detectors, charged particles produce *electron–hole pairs*. For the production of an electron–hole pair on the average 3.6 eV in silicon and 2.85 eV in germanium are required. This means that the number

of charge carriers produced in solid-state detectors is much larger compared to the production rate of electron–ion pairs in gases. Therefore, the statistical fluctuations in the number of produced charge carriers for a given energy loss is much smaller in solid-state detectors than in gaseous detectors.

The production of pairs of charge carriers for a given energy loss is a statistical process. If, on average, N charge-carrier pairs are produced one would naïvely expect this number to fluctuate according to Poisson statistics with an error of $\sqrt{N}$. Actually, the fluctuation around the average value is smaller by a factor $\sqrt{F}$ depending on the material; this was demonstrated for the first time by Fano [34]. If one considers the situation in detail, the origin of the *Fano factor* is clear. For a given energy deposit, the number of produced charge carriers is limited by energy conservation.

In the following, a formal justification for the Fano factor will be given [34, 35]. Let $E = E_{\text{total}}$ be the fixed energy deposited in a detector, e.g. by an X-ray photon or a stopping α particle. This energy is transferred in p steps to the detector medium, in general, in unequal portions E_p in each individual ionisation process. For each interaction step, m_p electron–ion pairs are produced. After N steps, the total energy is completely absorbed (Fig. 1.5).

Let

$m_p^{(\mathrm{e})} = \frac{E_p}{W}$ be the expected number of ionisations in the step p, and

$\overline{n}^{(\mathrm{e})} = \frac{E}{W}$ be the average expected number of the totally produced electron–ion pairs.

The quantity, which will finally describe the energy resolution, is

$$\sigma^2 = \left\langle (n - \overline{n})^2 \right\rangle \quad , \tag{1.35}$$

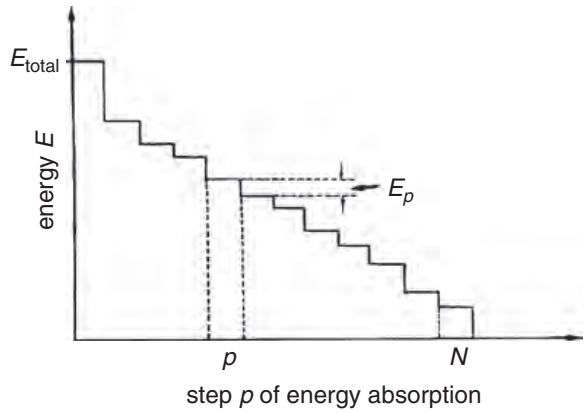

Fig. 1.5. Energy loss in N discrete steps with energy transfer E_p in the pth step [35].

where $\overline{n}$ is the average value over many experiments for fixed energy absorption:

$$\sigma^2 = \frac{1}{L}\sum_{k=1}^{L}(n_k - \overline{n})^2 \ . \tag{1.36}$$

That is, we perform L gedanken experiments, where in experiment k a total number n_k electron–ion pairs is produced. In experiment k the energy is transferred to the detector medium in N_k steps, where in the pth interval the number of produced electron–ion pairs is m_{pk};

$$n_k - \overline{n} = \sum_{p=1}^{N_k} m_{pk} - \frac{E}{W} = \sum_{p=1}^{N_k} m_{pk} - \frac{1}{W}\sum_{p=1}^{N_k} E_{pk} \ . \tag{1.37}$$

The second term in the sum constrains the statistical character of the charge-carrier production rate through energy conservation. Therefore, one would expect that the fluctuations are smaller compared to an unconstrained accidental energy-loss process.

The energy E is subdivided consequently into N_k discrete steps each with energy portion E_{pk}. If we introduce

$$\nu_{pk} = m_{pk} - \frac{E_{pk}}{W} \ , \tag{1.38}$$

it follows that

$$n_k - \overline{n} = \sum_{p=1}^{N_k} \nu_{pk} \ . \tag{1.39}$$

The variance for L experiments is given by

$$\sigma^2(n) = \frac{1}{L} \ \cdot \underbrace{\sum_{k=1}^{L}}_{L \text{ experiments}} \underbrace{\left(\sum_{p=1}^{N_k} \nu_{pk}\right)^2}_{\text{per experiment}} \ , \tag{1.40}$$

$$\sigma^2(n) = \frac{1}{L}\left(\sum_{k=1}^{L}\sum_{p=1}^{N_k} \nu_{pk}^2 + \sum_{k=1}^{L}\sum_{i\neq j}^{N_k} \nu_{ik}\nu_{jk}\right) \ . \tag{1.41}$$

Let us consider the mixed term at first:

$$\frac{1}{L}\sum_{k=1}^{L}\sum_{i\neq j}^{N_k} \nu_{ik}\nu_{jk} = \frac{1}{L}\sum_{k=1}^{L}\sum_{i=1}^{N_k} \nu_{ik}\left(\sum_{j=1}^{N_k} \nu_{jk} - \nu_{ik}\right) \ . \tag{1.42}$$

The last term in the bracket of Eq. (1.42) originates from the suppression of the product $\nu_{ik}\nu_{jk}$ for $i = j$, which is already contained in the quadratic terms.

For a given event k the average value

$$\overline{\nu}_k = \frac{1}{N_k} \sum_{j=1}^{N_k} \nu_{jk} \tag{1.43}$$

can be introduced. Using this quantity, one gets

$$\frac{1}{L} \sum_{k=1}^{L} \sum_{i \neq j}^{N_k} \nu_{ik}\nu_{jk} = \frac{1}{L} \sum_{k=1}^{L} N_k \overline{\nu}_k (N_k \overline{\nu}_k - \overline{\nu}_k) \ . \tag{1.44}$$

In this equation the last term ν_{ik} has been approximated by the average value $\overline{\nu}_k$. Under these conditions one obtains

$$\frac{1}{L} \sum_{k=1}^{L} \sum_{i \neq j}^{N_k} \nu_{ik}\nu_{jk} = \frac{1}{L} \sum_{k=1}^{L} N_k(N_k - 1)\overline{\nu}_k^2 = (\overline{N^2} - \overline{N})\overline{\nu}^2 \ , \tag{1.45}$$

if one assumes that N_k and $\overline{\nu}_k$ are uncorrelated, and $\overline{\nu}_k = \overline{\nu}$, if N_k is sufficiently large.

The average value of ν, however, vanishes according to Eq. (1.38), consequently the second term in Eq. (1.41) does not contribute. The remaining first term gives

$$\sigma^2(n) = \frac{1}{L} \sum_{k=1}^{L} \sum_{p=1}^{N_k} \nu_{pk}^2 = \frac{1}{L} \sum_{k=1}^{L} N_k \overline{\nu_k^2} = \overline{N\nu^2} = \overline{N} \cdot \overline{(m_p - E_p/W)^2} \ . \tag{1.46}$$

In this case m_p is the actually measured number of electron–ion pairs in the energy-absorption step p with energy deposit E_p.

Remembering that $\overline{N} = \frac{\overline{n}}{\overline{m}_p}$, leads to

$$\sigma^2(n) = \frac{\overline{(m_p - E_p/W)^2}}{\overline{m}_p} \, \overline{n} \ . \tag{1.47}$$

The variance of n consequently is

$$\sigma^2(n) = F \cdot \overline{n} \tag{1.48}$$

with the Fano factor

$$F = \frac{\overline{(m_p - E_p/W)^2}}{\overline{m}_p} \ . \tag{1.49}$$

Table 1.3. *Fano factors for typical detector materials at 300 K [35, 36]*

Absorber	F
Ar + 10% CH_4	≈ 0.2
Si	0.12
Ge	0.13
GaAs	0.10
Diamond	0.08

As a consequence, the energy resolution is improved by the factor $\sqrt{F}$ compared to Poisson fluctuations. However, it must be remembered that one has to distinguish between the occasional very large fluctuations of the energy loss (Landau fluctuations) in thin absorber layers and the fluctuation of the number of produced electron–ion pairs for a given fixed well-defined energy loss. This last case is true for all particles which deposit their total energy in the sensitive volume of the detector.

Table 1.3 lists some Fano factors for various substances at 300 K [35, 36]. The improvement on the energy resolution can be quite substantial.

1.1.4 Multiple scattering

A charged particle traversing matter will be scattered by the Coulomb potentials of nuclei and electrons. In contrast to the ionisation energy loss which is caused by collisions with atomic electrons, multiple-scattering processes are dominated by deflections in the Coulomb field of nuclei. This leads to a large number of scattering processes with very low deviations from the original path. The distribution of scattering angles due to multiple *Coulomb scattering* is described by *Molière's theory* [10–12, 37]. For small scattering angles it is normally distributed around the average scattering angle $\Theta = 0$. Larger scattering angles caused by collisions of charged particles with nuclei are, however, more frequent than expected from a Gaussian distribution [38].

The root mean square of the projected *scattering-angle distribution* is given by [10–12]

$$\Theta_{\text{rms}}^{\text{proj.}} = \sqrt{\langle \Theta^2 \rangle} = \frac{13.6\,\text{MeV}}{\beta c p} z \sqrt{\frac{x}{X_0}} \; [1 + 0.038 \ln(x/X_0)] \;, \qquad (1.50)$$

where p (in MeV/c) is the momentum, βc the velocity, and z the charge of the scattered particle. x/X_0 is the thickness of the scattering

medium, measured in units of the radiation length (see Sect. 1.1.5) [1, 39, 40]

$$X_0 = \frac{A}{4\alpha N_\mathrm{A} Z^2 r_e^2 \ln(183\ Z^{-1/3})}\ , \tag{1.51}$$

where Z and A are the atomic number and the atomic weight of the absorber, respectively.

Equation (1.50) is already an approximation. For most practical applications Eq. (1.50) can be further approximated for particles with $z = 1$ by

$$\Theta_\mathrm{rms}^\mathrm{proj.} = \sqrt{\langle\Theta^2\rangle} \approx \frac{13.6\,\mathrm{MeV}}{\beta cp}\sqrt{\frac{x}{X_0}}\ . \tag{1.52}$$

Equation (1.50) or (1.52) gives the root mean square of the projected distribution of the scattering angles. Such a projected distribution is, for example, of interest for detectors, which provide only a two-dimensional view of an event. The corresponding root mean square deviation for non-projected scattering angles is increased by factor $\sqrt{2}$ so that we have

$$\Theta_\mathrm{rms}^\mathrm{space} \approx \frac{19.2\,\mathrm{MeV}}{\beta cp}\ \sqrt{\frac{x}{X_0}}\ . \tag{1.53}$$

1.1.5 Bremsstrahlung

Fast charged particles lose, in addition to their ionisation loss, energy by interactions with the Coulomb field of the nuclei of the traversed medium. If the charged particles are decelerated in the Coulomb field of the nucleus, a fraction of their kinetic energy will be emitted in form of photons (*bremsstrahlung*).

The energy loss by bremsstrahlung for high energies can be described by [1]

$$-\frac{\mathrm{d}E}{\mathrm{d}x} \approx 4\alpha \cdot N_\mathrm{A} \cdot \frac{Z^2}{A} \cdot z^2 \left(\frac{1}{4\pi\varepsilon_0} \cdot \frac{e^2}{mc^2}\right)^2 \cdot E\ \ln\frac{183}{Z^{1/3}}\ . \tag{1.54}$$

In this equation

Z, A – are the atomic number and atomic weight of the medium,

z, m, E – are the charge number, mass and energy of the incident particle.

The bremsstrahlung energy loss of electrons is given correspondingly by

$$-\frac{\mathrm{d}E}{\mathrm{d}x} \approx 4\alpha N_{\mathrm{A}} \cdot \frac{Z^2}{A} r_e^2 \cdot E \ \ln \frac{183}{Z^{1/3}} \tag{1.55}$$

if $E \gg m_e c^2/\alpha Z^{1/3}$.

It should be pointed out that, in contrast to the ionisation energy loss, Eq. (1.11), the energy loss by bremsstrahlung is proportional to the energy of the particle and inversely proportional to the mass squared of the incident particles.

Because of the smallness of the electron mass, bremsstrahlung energy losses play an especially important rôle for electrons. For electrons ($z = 1,\ m = m_e$) Eq. (1.54) or Eq. (1.55), respectively, can be written in the following fashion:

$$-\frac{\mathrm{d}E}{\mathrm{d}x} = \frac{E}{X_0} \ . \tag{1.56}$$

This equation defines the *radiation length* X_0. An approximation for X_0 has already been given by Eq. (1.51).

The proportionality

$$X_0^{-1} \propto Z^2 \tag{1.57}$$

in Eq. (1.51) originates from the interaction of the incident particle with the Coulomb field of the target nucleus.

Bremsstrahlung, however, is also emitted in interactions of incident particles with the electrons of the target material. The cross section for this process follows closely the calculation of the bremsstrahlung energy loss on the target nucleus, the only difference being that for atomic target electrons the charge is always equal to unity, and therefore one obtains an additional contribution to the cross section, which is proportional to the number of target electrons, that is $\propto Z$. The cross section for bremsstrahlung must be extended by this term [9]. Therefore, the factor Z^2 in Eq. (1.51) must be replaced by $Z^2 + Z = Z(Z+1)$, which leads to a better description of the radiation length, accordingly,[†]

$$X_0 = \frac{A}{4\alpha N_{\mathrm{A}} Z(Z+1) r_e^2 \ln(183\ Z^{-1/3})}\ \{\mathrm{g/cm^2}\} \ . \tag{1.58}$$

In addition, one has to consider that the atomic electrons will screen the Coulomb field of the nucleus to a certain extent. If *screening effects*

[†] Units presented in curly brackets just indicate that the numerical result of the formula is given in the units shown in the brackets, i.e., in this case the radiation length comes out in $\mathrm{g/cm^2}$.

are taken into account, the radiation length can be approximated by [10–12]

$$X_0 = \frac{716.4 \cdot A[\mathrm{g/mol}]}{Z(Z+1)\ln(287/\sqrt{Z})} \ \mathrm{g/cm^2} \ . \tag{1.59}$$

The numerical results for the radiation length based on Eq. (1.59) deviate from those of Eq. (1.51) by a few per cent.

The radiation length X_0 is a property of the material. However, one can also define a radiation length for incident particles other than electrons. Because of the proportionality

$$X_0 \propto r_e^{-2} \tag{1.60}$$

and the relation

$$r_e = \frac{1}{4\pi\varepsilon_0} \cdot \frac{e^2}{m_e c^2} \ , \tag{1.61}$$

the 'radiation length', however, also has a dependence on the mass of the incident particle,

$$\tilde{X}_0 \propto m^2 \ . \tag{1.62}$$

The radiation lengths given in the literature, however, are always meant for electrons.

Integrating Eq. (1.54) or (1.56), respectively, leads to

$$E = E_0 \, \mathrm{e}^{-x/X_0} \ . \tag{1.63}$$

This function describes the exponential attenuation of the *energy* of charged particles by radiation losses. Note the distinction from the exponential attenuation of the *intensity* of a photon beam passing through matter (see Sect. 1.2, Eq. (1.92)).

The radiation length of a mixture of elements or a compound can be approximated by

$$X_0 = \frac{1}{\sum_{i=1}^{N} f_i / X_0^i} \ , \tag{1.64}$$

where f_i are the mass fractions of the components with the radiation length X_0^i.

Energy losses due to bremsstrahlung are proportional to the energy while ionisation energy losses beyond the minimum of ionisation are proportional to the logarithm of the energy. The energy, where these two interaction processes for electrons lead to equal energy losses, is called the *critical energy* E_c,

$$-\frac{\mathrm{d}E}{\mathrm{d}x}(E_\mathrm{c})\bigg|_\mathrm{ionisation} = -\frac{\mathrm{d}E}{\mathrm{d}x}(E_\mathrm{c})\bigg|_\mathrm{bremsstrahlung} \quad . \tag{1.65}$$

The energy distribution of bremsstrahlung photons follows a $1/E_\gamma$ law (E_γ – energy of the emitted photon). The photons are emitted preferentially in the forward direction ($\Theta_\gamma \approx m_e c^2/E$). In principle, the critical energy can be calculated from the Eqs. (1.11) and (1.54) using Eq. (1.65). Numerical values for the critical energy of electrons are given in the literature [9–11]. For solids the equation

$$E_\mathrm{c} = \frac{610\,\mathrm{MeV}}{Z + 1.24} \tag{1.66}$$

describes the critical energies quite satisfactorily [41]. Similar parametrisations for gases, liquids and solids are given in [12]. The critical energy is related to the radiation length by

$$\left(\frac{\mathrm{d}E}{\mathrm{d}x}\right) \cdot X_0 \approx E_\mathrm{c} \quad . \tag{1.67}$$

Table 1.4 lists the radiation lengths and critical energies for some materials [9–12]. The critical energy – as well as the radiation length – scales as the square of the mass of the incident particles. For muons ($m_\mu = 106\,\mathrm{MeV}/c^2$) in iron one obtains:

$$E_\mathrm{c}^\mu \approx E_\mathrm{c}^e \cdot \left(\frac{m_\mu}{m_e}\right)^2 = 890\,\mathrm{GeV} \quad . \tag{1.68}$$

1.1.6 Direct electron-pair production

Apart from bremsstrahlung losses, additional energy-loss mechanisms come into play, particularly at high energies. Electron–positron pairs can be produced by virtual photons in the Coulomb field of the nuclei. For high-energy muons this energy-loss mechanism is even more important than bremsstrahlung losses. The energy loss by *trident production* (e.g. like μ+nucleus $\rightarrow \mu + e^+ + e^-$ +nucleus) is also proportional to the energy and can be parametrised by

$$-\frac{\mathrm{d}E}{\mathrm{d}x}\bigg|_\mathrm{pair\ pr.} = b_\mathrm{pair}(Z, A, E) \cdot E \ ; \tag{1.69}$$

Table 1.4. *Radiation lengths and critical energies for some absorber materials [9–12]. The values for the radiation lengths agree with Eq. (1.59) within a few per cent. Only the experimental value for helium shows a somewhat larger deviation. The numerical results for the critical energies of electrons scatter quite significantly in the literature. The effective values for Z and A of mixtures and compounds can be calculated for A by $A_{eff} = \sum_{i=1}^{N} f_i A_i$, where f_i are the mass fractions of the components with atomic weight A_i. Correspondingly, one obtains the effective atomic numbers using Eqs. (1.59) and (1.64). Neglecting the logarithmic Z dependence in Eq. (1.59), Z_{eff} can be calculated from $Z_{eff} \cdot (Z_{eff} + 1) = \sum_{i=1}^{N} f_i Z_i (Z_i + 1)$, where f_i are the mass fractions of the components with charge numbers Z_i. For the practical calculation of an effective radiation length of a compound one determines first the radiation length of the contributing components and then determines the effective radiation length according to Eq. (1.64)*

Material	Z	A	X_0 [g/cm^2]	X_0 [cm]	E_c [MeV]
Hydrogen	1	1.01	61.3	731 000	350
Helium	2	4.00	94	530 000	250
Lithium	3	6.94	83	156	180
Carbon	6	12.01	43	18.8	90
Nitrogen	7	14.01	38	30 500	85
Oxygen	8	16.00	34	24 000	75
Aluminium	13	26.98	24	8.9	40
Silicon	14	28.09	22	9.4	39
Iron	26	55.85	13.9	1.76	20.7
Copper	29	63.55	12.9	1.43	18.8
Silver	47	109.9	9.3	0.89	11.9
Tungsten	74	183.9	6.8	0.35	8.0
Lead	82	207.2	6.4	0.56	7.40
Air	7.3	14.4	37	30 000	84
SiO_2	11.2	21.7	27	12	57
Water	7.5	14.2	36	36	83

the $b(Z, A, E)$ parameter varies only slowly with energy for high energies. For 100 GeV muons in iron the energy loss due to *direct electron-pair production* can be described by [25, 42, 43]

$$-\left.\frac{\mathrm{d}E}{\mathrm{d}x}\right|_{\text{pair pr.}} = 3 \cdot 10^{-6} \cdot \frac{E}{\text{MeV}} \; \frac{\text{MeV}}{\text{g/cm}^2} \;, \tag{1.70}$$

$$\text{i.e.} \; -\left.\frac{\mathrm{d}E}{\mathrm{d}x}\right|_{\text{pair pr.}} = 0.3 \; \frac{\text{MeV}}{\text{g/cm}^2} \;. \tag{1.71}$$

The spectrum of total energy of directly produced electron–positron pairs at high energy transfers is steeper than the spectrum of bremsstrahlung photons. High fractional energy transfers are therefore dominated by bremsstrahlung processes [25].

1.1.7 Energy loss by photonuclear interactions

Charged particles can interact inelastically via virtual gauge particles (in this case, photons) with nuclei of the absorber material, thereby losing energy (nuclear interactions).

In the same way as for energy losses through bremsstrahlung or direct electron-pair production, the energy loss by *photonuclear interactions* is proportional to the particle's energy,

$$-\left.\frac{\mathrm{d}E}{\mathrm{d}x}\right|_{\text{photonucl.}} = b_{\text{nucl.}}(Z, A, E) \cdot E \ . \tag{1.72}$$

For 100 GeV muons in iron the energy-loss parameter b is given by $b_{\text{nucl.}} = 0.4 \cdot 10^{-6}\,\text{g}^{-1}\,\text{cm}^2$ [25], i.e.,

$$-\left.\frac{\mathrm{d}E}{\mathrm{d}x}\right|_{\text{photonucl.}} = 0.04\ \frac{\text{MeV}}{\text{g/cm}^2} \ . \tag{1.73}$$

This energy loss is important for leptons and negligible for hadrons in comparison to direct nuclear interactions.

1.1.8 Total energy loss

In contrast to energy losses due to ionisation those by bremsstrahlung, direct electron-pair production and photonuclear interactions are characterised by large energy transfers with correspondingly large fluctuations. Therefore, it is somewhat problematic to speak of an average energy loss for these processes because extremely large fluctuations around this average value can occur [44, 45].

Nevertheless, the total energy loss of charged particles by the above mentioned processes can be parametrised by

$$\begin{aligned} -\left.\frac{\mathrm{d}E}{\mathrm{d}x}\right|_{\text{total}} &= -\left.\frac{\mathrm{d}E}{\mathrm{d}x}\right|_{\text{ionisation}} - \left.\frac{\mathrm{d}E}{\mathrm{d}x}\right|_{\text{brems.}} - \left.\frac{\mathrm{d}E}{\mathrm{d}x}\right|_{\text{pair pr.}} - \left.\frac{\mathrm{d}E}{\mathrm{d}x}\right|_{\text{photonucl.}} \\ &= a(Z, A, E) + b(Z, A, E) \cdot E \ , \end{aligned} \tag{1.74}$$

where $a(Z, A, E)$ describes the energy loss according to Eq. (1.11) and $b(Z, A, E)$ is the sum over the energy losses due to bremsstrahlung, direct electron-pair production and photonuclear interactions. The parameters

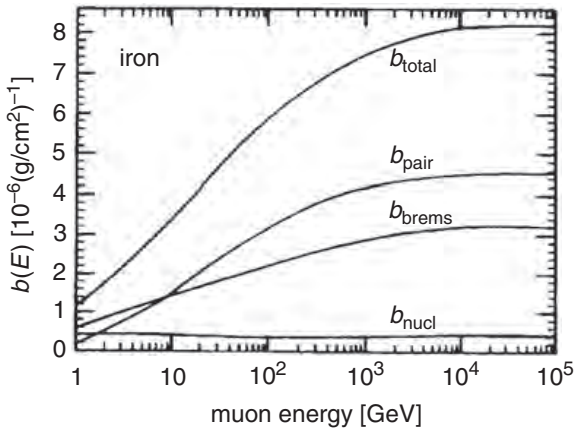

Fig. 1.6. Variation of the b parameters with energy for muons in iron. Plotted are the fractional energy losses by direct electron-pair production (b_{pair}), bremsstrahlung (b_{brems}), and photonuclear interactions (b_{nucl}), as well as their sum (b_{total}) [42].

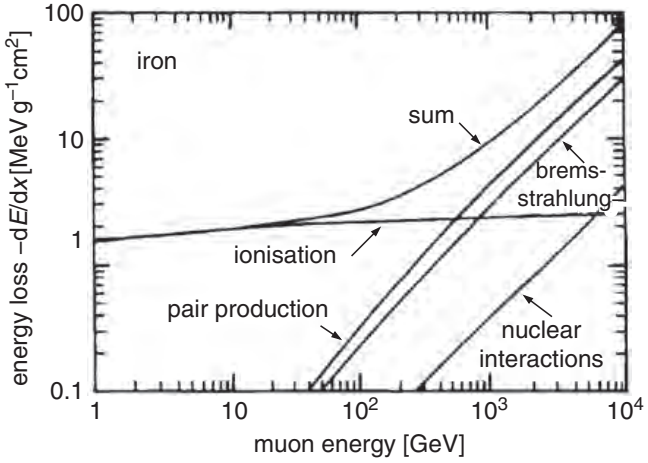

Fig. 1.7. Contributions to the energy loss of muons in iron [42].

a and b and their energy dependence for various particles and materials are given in the literature [46].

Figure 1.6 shows the b *parameters* and in Fig. 1.7 the various energy-loss mechanisms for muons in iron in their dependence on the muon energy are presented [42].

Up to energies of several hundred GeV the energy loss in iron due to ionisation and excitation is dominant. For energies in excess of several TeV direct electron-pair production and bremsstrahlung represent the main energy-loss processes. Photonuclear interactions contribute only at the 10% level. Since the energy loss due to these processes is proportional

to the muon's energy, this opens up the possibility of muon calorimetry by means of energy-loss sampling [47].

The dominance of the energy-proportional interaction processes over ionisation and excitation depends, of course, on the target material. For uranium this transition starts around several 100 GeV, while in hydrogen bremsstrahlung and direct electron-pair production prevail only at energies in excess of 10 TeV.

1.1.9 Energy–range relations for charged particles

Because of the different energy-loss mechanisms, it is nearly impossible to give a simple representation of the range of charged particles in matter. The definition of a range is in any case complicated because of the fluctuations of the energy loss by catastrophic energy-loss processes, i.e. by interactions with high energy transfers, and because of the multiple Coulomb scattering in the material, all of which lead to substantial range straggling. In the following, therefore, some empirical formulae are given, which are valid for certain particle species in fixed energy ranges.

Generally speaking, the range can be calculated from:

$$R = \int_E^{m_0c^2} \frac{\mathrm{d}E}{\mathrm{d}E/\mathrm{d}x} \ . \tag{1.75}$$

However, since the energy loss is a complicated function of the energy, in most cases approximations of this integral are used. For the determination of the range of low-energy particles, in particular, the difference between the total energy E and the kinetic energy E_{kin} must be taken into account, because only the kinetic energy can be transferred to the material.

For α particles with kinetic energies between $2.5\,\mathrm{MeV} \leq E_{\mathrm{kin}} \leq 20\,\mathrm{MeV}$ the range in air (15 °C, 760 Torr) can be described by [48]

$$R_\alpha = 0.31(E_{\mathrm{kin}}/\mathrm{MeV})^{3/2}\,\mathrm{cm} \ . \tag{1.76}$$

For rough estimates of the range of α particles in other materials one can use

$$R_\alpha = 3.2 \cdot 10^{-4} \frac{\sqrt{A/(\mathrm{g/mol})}}{\varrho/(\mathrm{g\,cm^{-3}})} \cdot R_{\mathrm{air}}\,\{\mathrm{cm}\} \tag{1.77}$$

(A atomic weight) [48]. The range of α particles in air is shown in Fig. 1.8.

For protons with kinetic energies between $0.6\,\mathrm{MeV} \leq E_{\mathrm{kin}} \leq 20\,\mathrm{MeV}$ the range in air [48] can be approximated by

$$R_p = 100 \cdot \left(\frac{E_{\mathrm{kin}}}{9.3\,\mathrm{MeV}}\right)^{1.8} \mathrm{cm} \ . \tag{1.78}$$

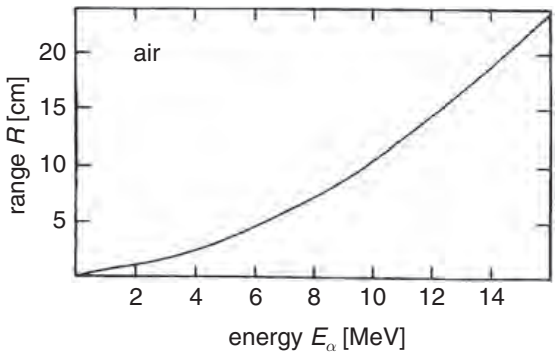

Fig. 1.8. Range of α particles in air [48].

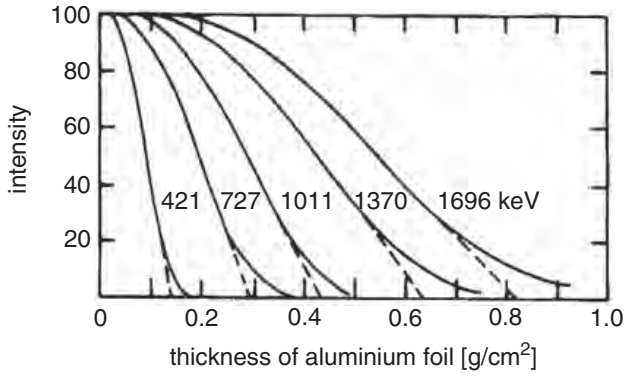

Fig. 1.9. Absorption of electrons in aluminium [49, 50].

The range of low-energy electrons ($0.5\,\mathrm{MeV} \leq E_{\mathrm{kin}} \leq 5\,\mathrm{MeV}$) in aluminium is described [48] by

$$R_e = 0.526\,(E_{\mathrm{kin}}/\mathrm{MeV} - 0.094)\,\mathrm{g/cm^2}\ . \tag{1.79}$$

Figure 1.9 shows the absorption of electrons in aluminium [49, 50]. Plotted is the fraction of electrons (with the energy E_{kin}), which penetrate through a certain absorber thickness.

This figure shows the difficulty in the definition of a range of a particle due to the pronounced range straggling, in this case mainly due to the fact that electrons will experience multiple scattering and will bremsstrahl in the absorber. For particles heavier than the electron the range is much better defined due to the reduced effect of multiple scattering ($\langle \Theta^2 \rangle \propto 1/p$). The extrapolation of the linear part of the curves shown in Fig. 1.9 to the intersection with the abscissa defines the *practical range* [50]. The range of electrons defined in this way is shown in Fig. 1.10 for various absorbers [50].

For higher energies the range of muons, pions and protons can be taken from Fig. 1.11 [12].

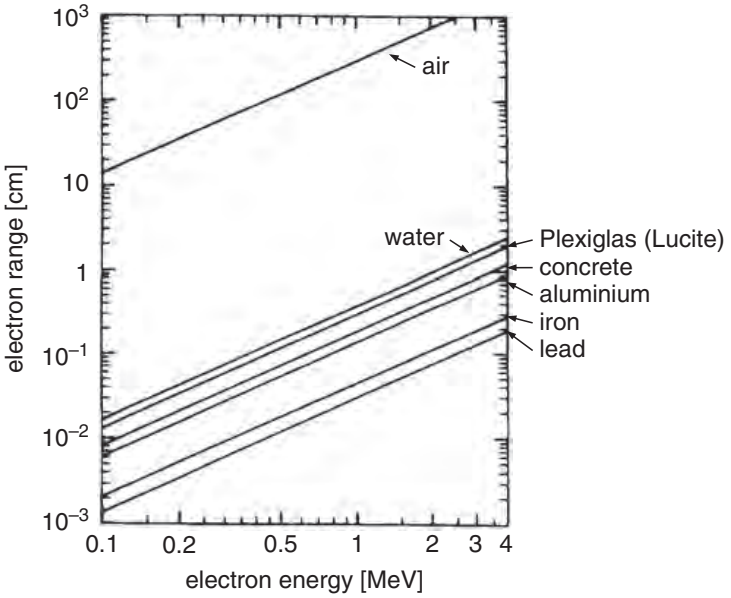

Fig. 1.10. Practical range of electrons in various materials [50].

The range of high-energy muons can be obtained by integrating Eq. (1.75), using Eqs. (1.74) and (1.11), and neglecting the logarithmic term in Eq. (1.11). This leads to

$$R_\mu(E_\mu) = \frac{1}{b} \ln\left(1 + \frac{b}{a} E_\mu\right) \ . \tag{1.80}$$

For 1 TeV muons in iron Eq. (1.80) yields

$$R_\mu(1\,\mathrm{TeV}) = 265\,\mathrm{m} \ . \tag{1.81}$$

A numerical integration for the range of muons in rock (standard rock with $Z = 11$, $A = 22$) yields for $E_\mu > 10\,\mathrm{GeV}$ [51]

$$R_\mu(E_\mu) = \left[\frac{1}{b} \ln(1 + \frac{b}{a} E_\mu)\right] \left(0.96 \frac{\ln E_{\mu,\mathrm{n}} - 7.894}{\ln E_{\mu,\mathrm{n}} - 8.074}\right) \tag{1.82}$$

with $a = 2.2\,\frac{\mathrm{MeV}}{\mathrm{g/cm^2}}$, $b = 4.4 \cdot 10^{-6}\,\mathrm{g^{-1}\,cm^2}$ and $E_{\mu,\mathrm{n}} = E_\mu/\mathrm{MeV}$. This energy–range dependence of muons in rock is shown in Fig. 1.12.

1.1.10 Synchrotron-radiation losses

There are further energy-loss processes of charged particles like *Cherenkov radiation*, *transition radiation* and *synchrotron radiation*. Cherenkov radiation and transition radiation will be discussed in those chapters where

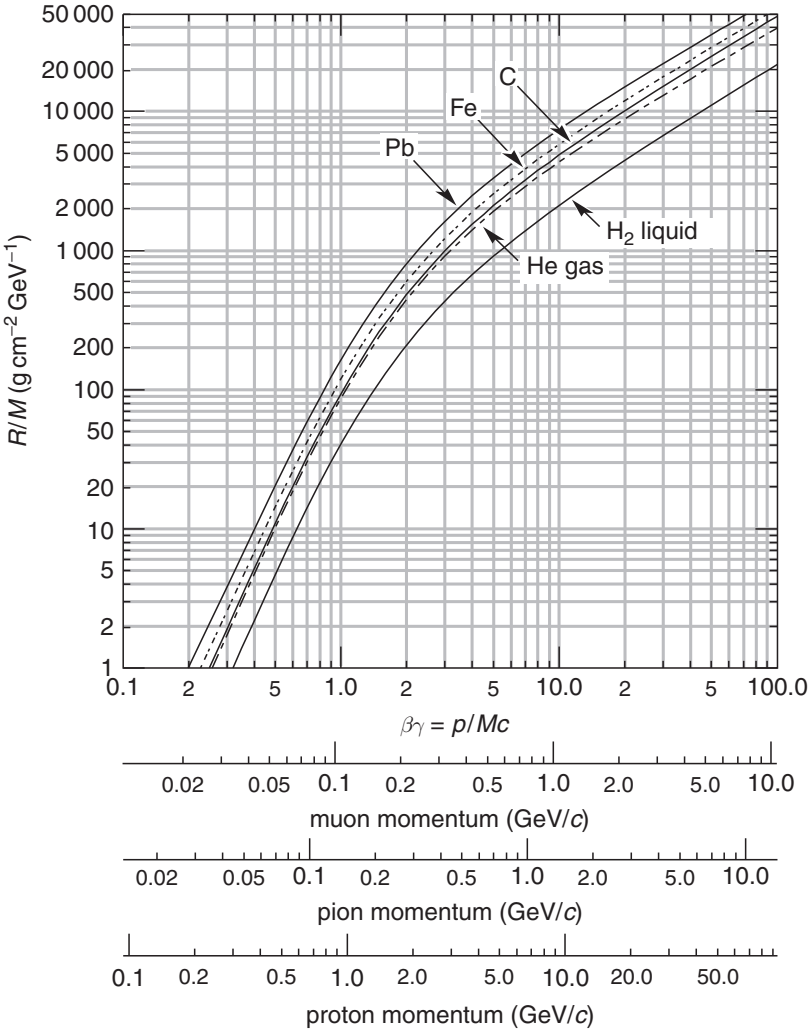

Fig. 1.11. Range of muons, pions and protons in liquid hydrogen, helium gas, carbon and lead [12].

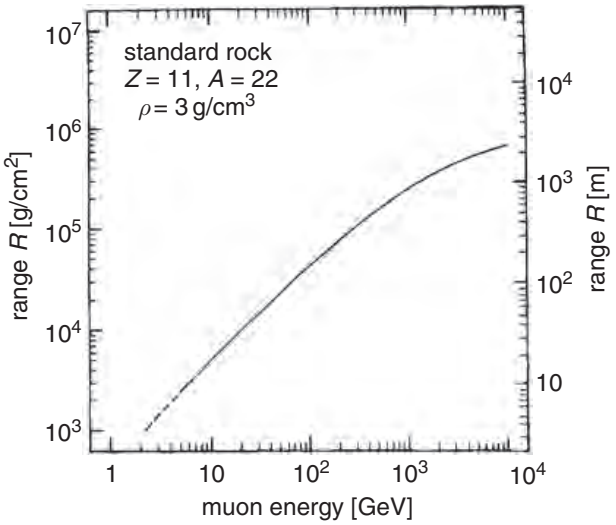

Fig. 1.12. Range of muons in rock [51].

Cherenkov detectors and transition-radiation detectors are described. Synchrotron-radiation losses are of general importance for charged-particle detection and acceleration, therefore a brief account on their essentials is given here.

Any charged particle accelerated in a straight line or on a curved path will emit electromagnetic radiation. This energy loss is particularly important for electrons deflected in a magnetic field.

The radiated power from an accelerated electron can be worked out from classical electrodynamics,

$$P = \frac{1}{4\pi\varepsilon_0}\frac{2e^2}{3c^3}a^2 \ , \tag{1.83}$$

where a is the acceleration. For the general case one has to consider relativistic effects. From

$$a = \frac{1}{m_0}\frac{\mathrm{d}p}{\mathrm{d}\tau} \tag{1.84}$$

and the proper time $\tau = t/\gamma$ one gets

$$a = \frac{1}{m_0}\cdot\gamma\frac{\mathrm{d}(\gamma m_0 v)}{\mathrm{d}t} = \gamma^2\frac{\mathrm{d}v}{\mathrm{d}t} = \gamma^2\cdot\frac{v^2}{r} \tag{1.85}$$

for an acceleration on a circle of radius r (v^2/r is the centrifugal acceleration).

This gives [40, 52]

$$P = \frac{1}{4\pi\varepsilon_0}\frac{2e^2}{3c^3}\gamma^4\frac{v^4}{r^2} = \frac{1}{6\pi\varepsilon_0}e^2c\frac{\gamma^4}{r^2} \tag{1.86}$$

for relativistic particles with $v \approx c$. For electrons one gets

$$P = \frac{e^2c}{6\pi\varepsilon_0}\left(\frac{E}{m_ec^2}\right)^4\cdot\frac{1}{r^2} = 4.22\cdot10^3\ \frac{E^4\ [\mathrm{GeV}^4]}{r^2\ [\mathrm{m}^2]}\,\mathrm{GeV/s}\ . \tag{1.87}$$

The energy loss per turn in a circular accelerator is

$$\Delta E = P\cdot\frac{2\pi r}{c} = \frac{e^2}{3\varepsilon_0}\frac{\gamma^4}{r} = 8.85\cdot10^{-5}\ \frac{E^4\ [\mathrm{GeV}^4]}{r\ [\mathrm{m}]}\,\mathrm{GeV}\ . \tag{1.88}$$

1.2 Interactions of photons

For the Large Electron–Positron collider LEP at CERN with a bending radius in the dipoles of 3100 m one obtains for a beam energy of 100 GeV

$$\Delta E = 2.85\,\mathrm{GeV\ per\ turn}\ , \tag{1.89}$$

while for the Large Hadron Collider LHC for proton beam energies of 7 TeV in the LEP tunnel one has

$$\Delta E = 8.85 \cdot 10^{-5} \cdot \left(\frac{m_e}{m_p}\right)^4 \frac{E^4\ [\mathrm{GeV}^4]}{r\ [m]}\,\mathrm{GeV} = 6 \cdot 10^{-6}\,\mathrm{GeV} = 6\,\mathrm{keV}\ . \tag{1.90}$$

The emitted synchrotron photons have a broad energy spectrum with a characteristic (critical) energy of

$$E_\mathrm{c} = \frac{3c}{2r}\hbar\gamma^3\ . \tag{1.91}$$

They are emitted into a forward cone with opening angle $\propto \frac{1}{\gamma}$. In particular, for electron accelerators the synchrotron-radiation loss is a severe problem for high-energy electrons. Therefore, electron accelerators for $E \gg 100\,\mathrm{GeV}$ have to be linear instead of circular.

On the other hand, the synchrotron radiation from circular electron machines is used for other fields of physics like solid state or atomic physics, biophysics or medical physics. Here the high *brilliance* of these machines, often augmented by extra bending magnets (*undulators* and *wigglers*) provides excellent opportunities for structure analysis of a large variety of samples. Also the dynamical behaviour of fast biological processes can be investigated.

1.2 Interactions of photons

Photons are detected indirectly via interactions in the medium of the detector. In these processes charged particles are produced which are recorded through their subsequent ionisation in the sensitive volume of the detector. Interactions of photons are fundamentally different from ionisation processes of charged particles because in every photon interaction, the photon is either completely absorbed (*photoelectric effect*, *pair production*) or scattered through a relatively large angle (*Compton effect*). Since the absorption or scattering is a statistical process, it is impossible to define a range for γ rays. A photon beam is attenuated exponentially in matter according to

$$I = I_0\ \mathrm{e}^{-\mu x}\ . \tag{1.92}$$

The *mass attenuation coefficient* μ is related to the cross sections for the various interaction processes of photons according to

$$\mu = \frac{N_\mathrm{A}}{A} \sum_i \sigma_i \ , \tag{1.93}$$

where σ_i is the atomic cross section for the process i, A the atomic weight and N_A the Avogadro number.

The mass attenuation coefficient (according to Eq. (1.93) given per g/cm^2) depends strongly on the photon energy. For low energies (100 keV $\geq E_\gamma \geq$ ionisation energy) the photoelectric effect dominates,

$$\gamma + \mathrm{atom} \ \rightarrow \ \mathrm{atom}^+ + e^- \ . \tag{1.94}$$

In the range of medium energies ($E_\gamma \approx 1\,\mathrm{MeV}$) the Compton effect, which is the scattering of photons off quasi-free atomic electrons,

$$\gamma + e^- \ \rightarrow \ \gamma + e^- \ , \tag{1.95}$$

has the largest cross section, and at higher energies ($E_\gamma \gg 1\,\mathrm{MeV}$) the cross section for pair production dominates,

$$\gamma + \mathrm{nucleus} \ \rightarrow \ e^+ + e^- + \mathrm{nucleus} \ . \tag{1.96}$$

The length x in Eq. (1.92) is an area density with the unit g/cm^2. If the length is measured in cm, the mass attenuation coefficient μ must be divided by the density ϱ of the material.

1.2.1 Photoelectric effect

Atomic electrons can absorb the energy of a photon completely, while – because of momentum conservation – this is not possible for free electrons. The absorption of a photon by an atomic electron requires a third collision partner which in this case is the atomic nucleus. The cross section for absorption of a photon of energy E_γ in the K shell is particularly large ($\approx$ 80% of the total cross section), because of the proximity of the third collision partner, the atomic nucleus, which takes the recoil momentum. The total photoelectric cross section in the non-relativistic range away from the absorption edges is given in the non-relativistic *Born approximation* by [53]

$$\sigma^\mathrm{K}_\mathrm{photo} = \left(\frac{32}{\varepsilon^7}\right)^{1/2} \alpha^4 \cdot Z^5 \cdot \sigma^e_\mathrm{Th} \ \ \{\mathrm{cm}^2/\mathrm{atom}\} \ , \tag{1.97}$$

where $\varepsilon = E_\gamma / m_e c^2$ is the reduced photon energy and $\sigma^e_\mathrm{Th} = \frac{8}{3}\,\pi\, r_e^2 = 6.65 \cdot 10^{-25}\,\mathrm{cm}^2$ is the *Thomson cross section* for elastic scattering of

photons on electrons. Close to the absorption edges, the energy dependence of the cross section is modified by a function $f(E_\gamma, E_\gamma^{\mathrm{edge}})$. For higher energies ($\varepsilon \gg 1$) the energy dependence of the cross section for the photoelectric effect is much less pronounced,

$$\sigma_{\mathrm{photo}}^{\mathrm{K}} = 4\pi r_e^2 Z^5 \alpha^4 \cdot \frac{1}{\varepsilon} \ . \tag{1.98}$$

In Eqs. (1.97) and (1.98) the Z dependence of the cross section is approximated by Z^5. This indicates that the photon does not interact with an isolated atomic electron. Z-dependent corrections, however, cause σ_{photo} to be a more complicated function of Z. In the energy range between $0.1\,\mathrm{MeV} \leq E_\gamma \leq 5\,\mathrm{MeV}$ the exponent of Z varies between 4 and 5.

As a consequence of the photoelectric effect in an inner shell (e.g. of the K shell) the following secondary effects may occur. If the free place, e.g. in the K shell, is filled by an electron from a higher shell, the energy difference between those two shells can be liberated in the form of X rays of characteristic energy. The energy of characteristic X rays is given by *Moseley's law*,

$$E = Ry\,(Z-1)^2 \left(\frac{1}{n^2} - \frac{1}{m^2}\right) \ , \tag{1.99}$$

where Ry ($= 13.6\,\mathrm{eV}$) is *Rydberg's constant* and n and m are the principal quantum numbers characterising the atomic shells. For a level transition from the L shell ($m = 2$) to the K shell ($n = 1$) one gets

$$E(\mathrm{K}_\alpha) = \frac{3}{4} Ry\,(Z-1)^2 \ . \tag{1.100}$$

However, this energy difference can also be transferred to an electron of the *same* atom. If this energy is larger than the binding energy of the shell in question, a further electron can leave the atom (Auger effect, *Auger electron*). The energy of these Auger electrons is usually quite small compared to the energy of the primary photoelectrons.

If the photoionisation occurs in the K shell (binding energy B_{K}), and if the hole in the K shell is filled up by an electron from the L shell (binding energy B_{L}), the excitation energy of the atom ($B_{\mathrm{K}} - B_{\mathrm{L}}$) can be transferred to an L electron. If $B_{\mathrm{K}} - B_{\mathrm{L}} > B_{\mathrm{L}}$, the L electron can leave the atomic shell with an energy $B_{\mathrm{K}} - 2B_{\mathrm{L}}$ as an Auger electron.

1.2.2 Compton effect

The Compton effect is the scattering of photons off quasi-free atomic electrons. In the treatment of this interaction process, the binding energy of

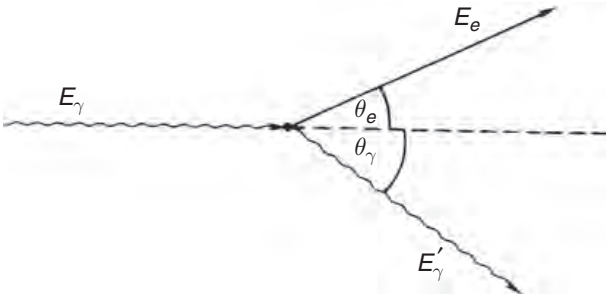

Fig. 1.13. Definition of kinematic variables in Compton scattering.

the atomic electrons is neglected. The differential probability of Compton scattering $\phi_{\rm c}(E_\gamma, E'_\gamma)\,{\rm d}E'_\gamma$ for $m_e c^2/2 < E'_\gamma < E_\gamma$ is given by the Klein–Nishina formula

$$\phi_{\rm c}(E_\gamma, E'_\gamma)\,{\rm d}E'_\gamma = \pi r_e^2 \frac{N_{\rm A} Z}{A} \frac{m_e c^2}{E_\gamma} \frac{{\rm d}E'_\gamma}{E'_\gamma} \left[1 + \left(\frac{E'_\gamma}{E_\gamma}\right)^2 - \frac{E'_\gamma}{E_\gamma} \sin^2\theta_\gamma\right] \ , \tag{1.101}$$

where θ_γ is the scattering angle of the photon in the laboratory system (see Fig. 1.13) and E_γ, E'_γ are the energies of the incident and scattered photon [54, 55]. The total cross section for Compton scattering per electron is given by [55]

$$\sigma_{\rm c}^e = 2\pi r_e^2 \left[\left(\frac{1+\varepsilon}{\varepsilon^2}\right)\left\{\frac{2(1+\varepsilon)}{1+2\varepsilon} - \frac{1}{\varepsilon}\ln(1+2\varepsilon)\right\} + \frac{1}{2\varepsilon}\ln(1+2\varepsilon) - \frac{1+3\varepsilon}{(1+2\varepsilon)^2}\right] \ \{{\rm cm}^2/{\rm electron}\} \ , \tag{1.102}$$

where

$$\varepsilon = \frac{E_\gamma}{m_e c^2} \ . \tag{1.103}$$

The angular and energy distributions of Compton electrons are discussed in great detail in R.D. Evans [56] and G. Hertz [48]. For the energy spectrum of Compton electrons one gets

$$\frac{{\rm d}\sigma_{\rm c}^e}{{\rm d}E_{\rm kin}} = \frac{{\rm d}\sigma_{\rm c}^e}{{\rm d}\Omega} \frac{2\pi}{\varepsilon^2 m_e c^2} \left[\frac{(1+\varepsilon)^2 - \varepsilon^2\cos^2\theta_e}{(1+\varepsilon)^2 - \varepsilon(2+\varepsilon)\cos^2\theta_e}\right]^2 \ , \tag{1.104}$$

where

$$\frac{{\rm d}\sigma_{\rm c}^e}{{\rm d}\Omega} = \frac{r_e^2}{2}\left(\frac{E'_\gamma}{E_\gamma}\right)^2 \left[\frac{E_\gamma}{E'_\gamma} - \frac{E'_\gamma}{E_\gamma} - \sin^2\theta_\gamma\right] \ . \tag{1.105}$$

For Compton scattering off atoms the cross section is increased by the factor Z, because there are exactly Z electrons as possible scattering partners in an atom; consequently $\sigma_{\rm c}^{\rm atomic} = Z \cdot \sigma_{\rm c}^{e}$.

At high energies the energy dependence of the Compton-scattering cross section can be approximated by [57]

$$\sigma_{\rm c}^{e} \propto \frac{\ln \varepsilon}{\varepsilon} \quad . \tag{1.106}$$

The ratio of scattered to incident photon energy is given by

$$\frac{E'_\gamma}{E_\gamma} = \frac{1}{1+\varepsilon(1-\cos\theta_\gamma)} \quad . \tag{1.107}$$

For *backscattering* ($\theta_\gamma = \pi$) the energy transfer to the electron reaches a maximum value, leading to a ratio of scattered to incident photon energy of

$$\frac{E'_\gamma}{E_\gamma} = \frac{1}{1+2\varepsilon} \quad . \tag{1.108}$$

The scattering angle of the electron with respect to the direction of the incident photon can be obtained from (see Problem 1.5)

$$\cot\theta_e = (1+\varepsilon)\tan\frac{\theta_\gamma}{2} \quad . \tag{1.109}$$

Because of momentum conservation the scattering angle of the electron, θ_e, can never exceed $\pi/2$.

In Compton-scattering processes only a fraction of the photon energy is transferred to the electron. Therefore, one defines an energy scattering cross section

$$\sigma_{\rm cs} = \frac{E'_\gamma}{E_\gamma} \cdot \sigma_{\rm c}^{e} \tag{1.110}$$

and subsequently an energy-absorption cross section

$$\sigma_{\rm ca} = \sigma_{\rm c}^{e} - \sigma_{\rm cs} \quad . \tag{1.111}$$

The latter is relevant for absorption processes and is related to the probability that an energy $E_{\rm kin} = E_\gamma - E'_\gamma$ is transferred to the target electron.

In passing, it should be mentioned that in addition to the normal Compton scattering of photons on target electrons at rest, *inverse Compton scattering* also exists. In this case, an energetic electron collides with a low-energy photon and transfers a fraction of its kinetic energy to the

photon which is blueshifted to higher frequencies. This inverse Compton-scattering process plays an important rôle, e.g. in astrophysics. Starlight photons (eV range) can be shifted in this way by collisions with energetic electrons into the X-ray (keV) or gamma (MeV) range. Laser photons backscattered from high-energy electron beams also provide energetic γ beams which are used in accelerator experiments [58].

Naturally, Compton scattering does not only occur with electrons, but also for other charged particles. For the measurement of photons in particle detectors, however, Compton scattering off atomic electrons is of special importance.

1.2.3 Pair production

The production of electron–positron pairs in the Coulomb field of a nucleus is only possible if the photon energy exceeds a certain threshold. This threshold energy is given by the rest masses of two electrons plus the recoil energy which is transferred to the nucleus. From energy and momentum conservation, this threshold energy can be calculated to be

$$E_\gamma \geq 2m_e c^2 + 2\frac{m_e^2}{m_{\text{nucleus}}}c^2 \ . \tag{1.112}$$

Since $m_{\text{nucleus}} \gg m_e$, the effective threshold can be approximated by

$$E_\gamma \geq 2m_e c^2 \ . \tag{1.113}$$

If, however, the electron–positron pair production proceeds in the Coulomb field of an electron, the threshold energy is

$$E_\gamma \geq 4m_e c^2 \ . \tag{1.114}$$

Electron–positron pair production in the Coulomb field of an electron is, however, strongly suppressed compared to pair production in the Coulomb field of the nucleus.

In the case that the nuclear charge is not screened by atomic electrons, (for low energies the photon must come relatively close to the nucleus to make pair production probable, which means that the photon sees only the 'naked' nucleus),

$$1 \ll \varepsilon < \frac{1}{\alpha Z^{1/3}} \ , \tag{1.115}$$

the pair-production cross section is given by [1]

$$\sigma_{\text{pair}} = 4\alpha r_e^2 Z^2 \left(\frac{7}{9}\ln 2\varepsilon - \frac{109}{54}\right) \ \{\text{cm}^2/\text{atom}\} \ ; \tag{1.116}$$

for complete screening of the nuclear charge, however, $\left(\varepsilon \gg \frac{1}{\alpha Z^{1/3}}\right)$ [1]

$$\sigma_{\text{pair}} = 4\alpha r_e^2 Z^2 \left(\frac{7}{9} \ln \frac{183}{Z^{1/3}} - \frac{1}{54}\right) \ \{\text{cm}^2/\text{atom}\} \ . \tag{1.117}$$

(At high energies pair production can also proceed at relatively large impact parameters of the photon with a respect to the nucleus. But in this case the screening of the nuclear charge by the atomic electrons must be taken into account.)

For large photon energies, the pair-production cross section approaches an energy-independent value which is given by Eq. (1.117). Neglecting the small term $\frac{1}{54}$ in the bracket of this equation, this asymptotic value is given by

$$\sigma_{\text{pair}} \approx \frac{7}{9} \, 4\alpha \, r_e^2 Z^2 \ln \frac{183}{Z^{1/3}} \approx \frac{7}{9} \cdot \frac{A}{N_{\text{A}}} \cdot \frac{1}{X_0} \ , \tag{1.118}$$

see Eq. (1.51).

The partition of the energy between the produced electrons and positrons is uniform at low and medium energies and becomes slightly asymmetric at large energies. The differential cross section for the creation of a positron of total energy between E_+ and $E_+ + \mathrm{d}E_+$ with an electron of total energy E_- is given by [53]

$$\frac{\mathrm{d}\sigma_{\text{pair}}}{\mathrm{d}E_+} = \frac{\alpha r_e^2}{E_\gamma - 2m_e c^2} \cdot Z^2 \cdot f(\varepsilon, Z) \ \{\text{cm}^2/(\text{MeV} \cdot \text{atom})\} \ . \tag{1.119}$$

$f(\varepsilon, Z)$ is a dimensionless, non-trivial function of ε and Z. The trivial Z^2 dependence of the cross section is, of course, already considered in a factor separated from $f(\varepsilon, Z)$. Therefore, $f(\varepsilon, Z)$ depends only weakly (logarithmically) on the atomic number of the absorber, see Eq. (1.117). $f(\varepsilon, Z)$ varies with Z only by few per cent [14]. The dependence of this function on the *energy-partition parameter*

$$x = \frac{E_+ - m_e c^2}{E_\gamma - 2m_e c^2} = \frac{E_+^{\text{kin}}}{E_{\text{pair}}^{\text{kin}}} \tag{1.120}$$

for average Z values is shown in Fig. 1.14 for various parameters ε [14, 59, 60]. The curves shown in Fig. 1.14 do not just include the pair production on the nucleus, but also the pair-production probability on atomic electrons ($\propto Z$), so that the Z^2 dependence of the pair-production cross section, Eq. (1.119), is modified to $Z(Z+1)$ in a similar way as was argued when the electron-bremsstrahlung process was presented, see Eq. (1.58). The angular distribution of the produced electrons is quite narrow with a characteristic opening angle of $\Theta \approx m_e c^2 / E_\gamma$.

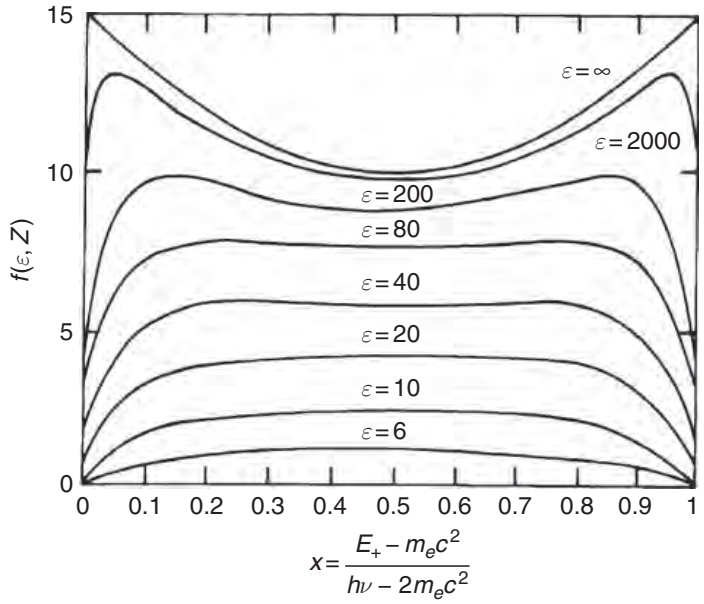

Fig. 1.14. Form of the energy-partition function $f(\varepsilon, Z, x)$ with $\varepsilon = E_\gamma/m_e c^2$ as parameter. The total pair-production cross section is given by the area under the corresponding curve in units of $Z(Z+1)\alpha r_e^2$ [14, 59, 60].

1.2.4 Total photon absorption cross section

The total mass attenuation coefficient, which is related to the cross sections according to Eq. (1.93), is shown in Figs. 1.15–1.18 for the absorbers water, air, aluminium and lead [48, 56, 61, 62].

Since Compton scattering plays a special rôle for photon interactions, because only part of the photon energy is transferred to the target electron, one has to distinguish between the *mass attenuation coefficient* and the *mass absorption coefficient*. The mass attenuation coefficient $\mu_{\rm cs}$ is related to the Compton-energy scattering cross section $\sigma_{\rm cs}$, see Eq. (1.110), according to Eq. (1.93). Correspondingly, the mass absorption coefficient $\mu_{\rm ca}$ is calculated from the energy absorption cross section $\sigma_{\rm ca}$, Eq. (1.111) and Eq. (1.93). For various absorbers the Compton-scattering cross sections, or absorption coefficients shown in Figs. 1.15–1.18, have been multiplied by the atomic number of the absorber, since the Compton-scattering cross section, Eq. (1.102), given by the Klein–Nishina formula is valid per electron, but in this case, the atomic cross sections are required.

Ranges in which the individual photon interaction processes dominate, are plotted in Fig. 1.19 as a function of the photon energy and the atomic number of the absorber [14, 50, 53].

Further interactions of photons (photonuclear interactions, *photon–photon scattering*, etc.) are governed by extremely low cross sections.

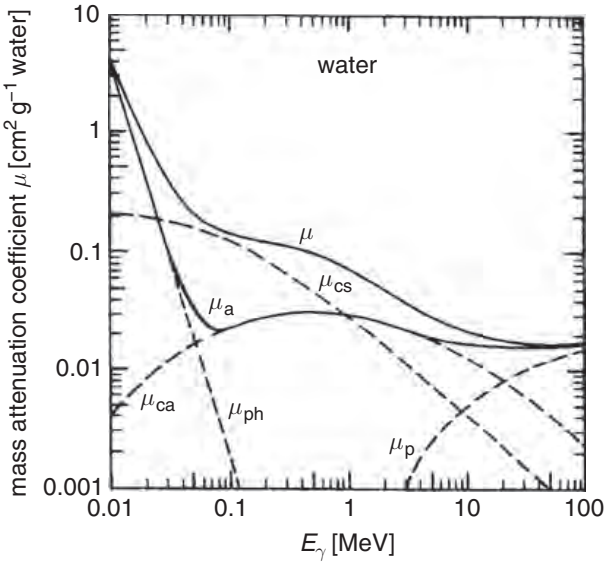

Fig. 1.15. Energy dependence of the mass attenuation coefficient μ and mass absorption coefficient μ_a for photons in water [48, 56, 61, 62]. μ_{ph} describes the photoelectric effect, μ_{cs} the Compton scattering, μ_{ca} the Compton absorption and μ_p the pair production. μ_a is the total mass absorption coefficient ($\mu_a = \mu_{ph} + \mu_p + \mu_{ca}$) and μ is the total mass attenuation coefficient ($\mu = \mu_{ph} + \mu_p + \mu_c$, where $\mu_c = \mu_{cs} + \mu_{ca}$).

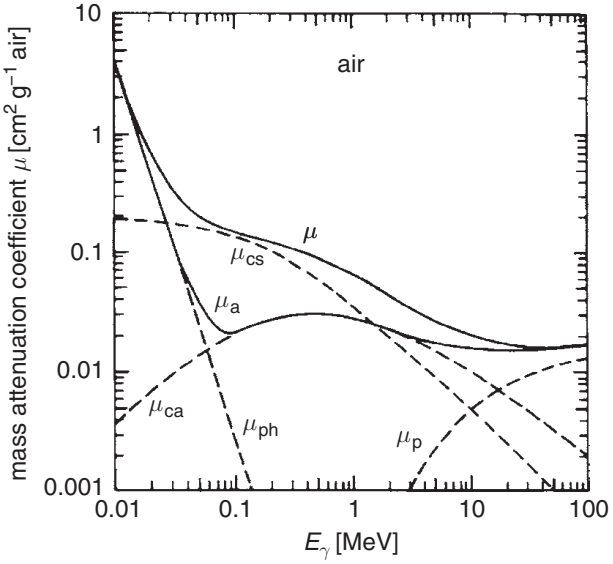

Fig. 1.16. Energy dependence of the mass attenuation coefficient μ and mass absorption coefficient μ_a for photons in air [48, 56, 61, 62].

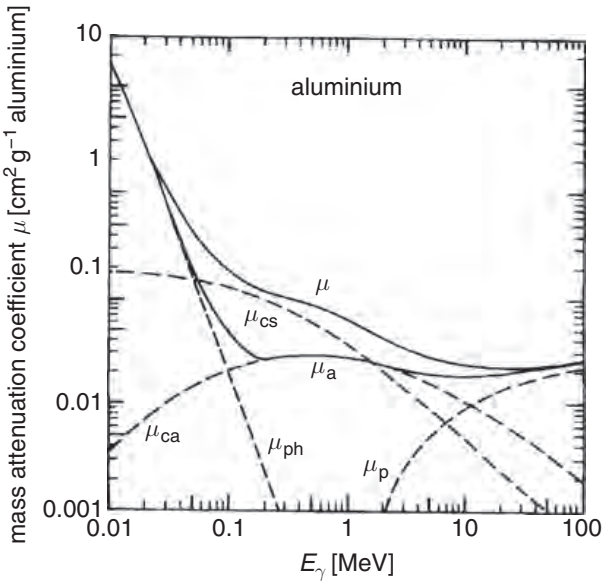

Fig. 1.17. Energy dependence of the mass attenuation coefficient μ and mass absorption coefficient μ_a for photons in aluminium [48, 56, 61, 62].

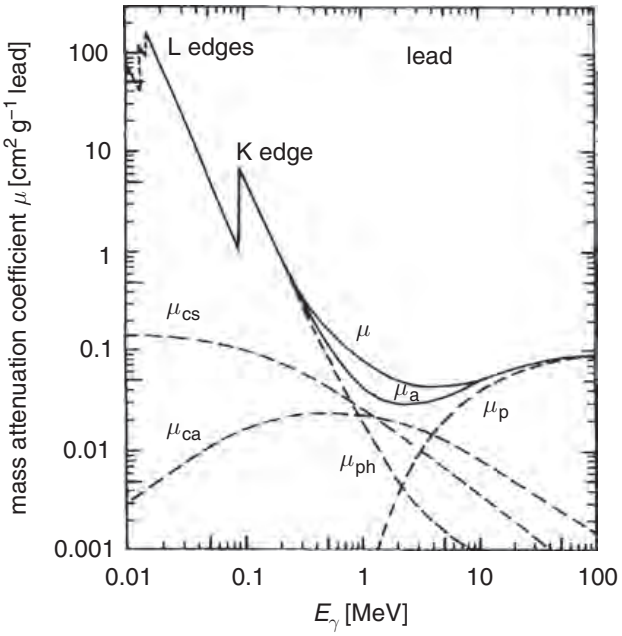

Fig. 1.18. Energy dependence of the mass attenuation coefficient μ and mass absorption coefficient μ_a for photons in lead [48, 56, 61, 62].

Therefore, these processes are of little importance for the detection of photons. However, these processes are of large interest in elementary particle physics and particle astrophysics.

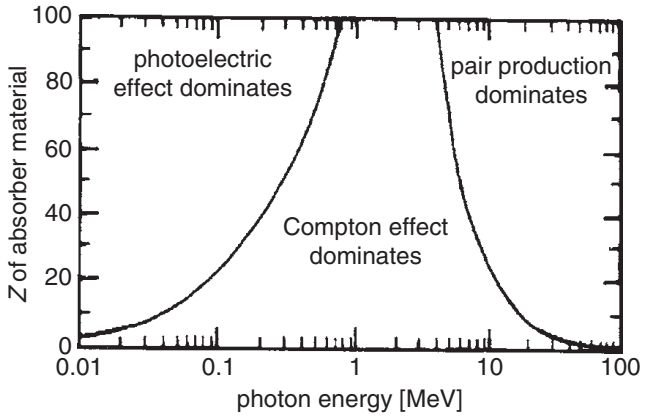

Fig. 1.19. Ranges in which the photoelectric effect, Compton effect and pair production dominate as a function of the photon energy and the target charge number Z [14, 50, 53].

Giant Photonuclear Resonance Neutrons [1]

Neutron production can be expected to occur in any material irradiated by electrons in which bremsstrahlung photons above the material-dependent threshold are produced. This neutron production threshold varies from 10 to 19 MeV for light nuclei and 4 to 6 MeV for heavy nuclei. Thresholds of 2.23 MeV for deuterium and 1.67 MeV for beryllium are exceptions. Other exceptions exist for isolated target nuclei and should be verified individually, perhaps using the online resources of the U. S. National Nuclear Data Center (NNDC 2018). Between this threshold and approximately 30 MeV, a production mechanism known as the giant photonuclear resonance, a (γ,n) reaction, is the most important source of neutron emission from material. The notation (γ,n) is that common in nuclear physics where the symbol for the incoming particle, here γ for a photon, is on the left while the symbol representative of the outgoing particle, here n for the neutron, is on the right within the parentheses.

Swanson (1979a) has given a detailed description of this process that is summarized here. A simple picture of this phenomenon is that the electric field of the photon produced by bremsstrahlung transfers its energy to the nucleus by inducing an oscillation in which the protons as a group move oppositely to the neutrons as a group. This process has a broad maximum cross section at photon energies ko between about 20-23 MeV for materials having mass numbers A less than about 40. For heavier targets, the peak is at an energy of approximately ko=80A^-1/3 MeV. Fassò et al. (1990) have provided a great deal of data on the relevant cross sections. It turns out that the yield Y of giant resonance neutrons at energies above approximately 2ko is nearly independent of energy and nearly proportional to the beam power.

[1] from 'ACCELERATOR RADIATION PHYSICS FOR PERSONNEL AND ENVIRONMENTAL PROTECTION', Fermilab Report TM-1834

References

[1] B. Rossi, *High Energy Particles*, Prentice-Hall, Englewood Cliffs (1952)

[2] B. Sitar, G.I. Merson, V.A. Chechin & Yu.A. Budagov, *Ionization Measurements in High Energy Physics* (in Russian), Energoatomizdat, Moskau (1988)

[3] B. Sitar, G.I. Merson, V.A. Chechin & Yu.A. Budagov, *Ionization Measurements in High Energy Physics*, Springer Tracts in Modern Physics, Vol. 124, Springer, Berlin/Heidelberg (1993)

[4] H.A. Bethe, Theorie des Durchgangs schneller Korpuskularstrahlen durch Materie, *Ann. d. Phys.* **5** (1930) 325–400

[5] H.A. Bethe, Bremsformel für Elektronen mit relativistischen Geschwindigkeiten, *Z. Phys.* **76** (1932) 293–9

[6] F. Bloch, Bremsvermögen von Atomen mit mehreren Elektronen, *Z. Phys.* **81** (1933) 363–76

[7] R.M. Sternheimer & R.F. Peierls, General Expression for the Density Effect for the Ionization Loss of Charged Particles, *Phys. Rev.* **B3** (1971) 3681–92

[8] E.A. Uehling, Penetration of Heavy Charged Particles in Matter, *Ann. Rev. Nucl. Part. Sci.* **4** (1954) 315–50

[9] S. Hayakawa, *Cosmic Ray Physics*, John Wiley & Sons Inc. (Wiley Interscience) (1969)

[10] Particle Data Group, Review of Particle Properties, *Phys. Lett.* **239** (1990) 1–516

[11] Particle Data Group, Review of Particle Properties, *Phys. Rev.* **D45** (1992) 1–574; Particle Data Group, *Phys. Rev.* **D46** (1992) 5210-0 (Errata)

[12] Particle Data Group, Review of Particle Physics, S. Eidelman *et al.*, *Phys. Lett.* **B592 Vol. 1–4** (2004) 1–1109; W.-M. Yao *et al.*, *J. Phys.* **G33** (2006) 1–1232; http://pdg.lbl.gov

[13] C. Serre, *Evaluation de la Perte D'Energie et du Parcours de Particules Chargées Traversant un Absorbant Quelconque*, CERN **67-5** (1967)

[14] P. Marmier, *Kernphysik I*, Verlag der Fachvereine, Zürich (1977)

[15] L. Landau, On the Energy Loss of Fast Particles by Ionization, *J. Phys. USSR* **8** (1944) 201–5

[16] R.S. Kölbig, *Landau Distribution*, CERN Program Library G 110, CERN Program Library Section (1985)

[17] P.V. Vavilov, Ionization Losses of High Energy Heavy Particles, *Sov. Phys. JETP* **5** (1957) 749–51

[18] R. Werthenbach, *Elektromagnetische Wechselwirkungen von 200 GeV Myonen in einem Streamerrohr-Kalorimeter*, Diploma Thesis, University of Siegen (1987)

[19] S. Behrends & A.C. Melissinos, *Properties of Argon–Ethane/Methane Mixtures for Use in Proportional Counters*, University of Rochester, Preprint UR-776 (1981)

[20] J.E. Moyal, Theory of Ionization Fluctuations, *Phil. Mag.* **46** (1955), 263–80

[21] R.K. Bock *et al.* (eds.), *Formulae and Methods in Experimental Data Evaluation*, General Glossary, Vol. 1, European Physical Society, CERN/Geneva (1984) 1–231

[22] Y. Iga *et al.*, Energy Loss Measurements for Charged Particles and a New Approach Based on Experimental Results, *Nucl. Instr. Meth.* **213** (1983) 531–7

[23] K. Affholderbach *et al.*, Performance of the New Small Angle Monitor for BAckground (SAMBA) in the ALEPH Experiment at CERN, *Nucl. Instr. Meth.* **A410** (1998) 166–75

[24] S.I. Striganov, Ionization Straggling of High Energy Muons in Thick Absorbers, *Nucl. Instr. Meth.* **A322** (1992) 225–30

[25] C. Grupen, Electromagnetic Interactions of High Energy Cosmic Ray Muons, *Fortschr. der Physik* **23** (1976) 127–209

[26] U. Fano, Penetration of Photons, Alpha Particles and Mesons, *Ann. Rev. Nucl. Sci.* **13** (1963) 1–66

[27] G. Musiol, J. Ranft, R. Reif & D. Seeliger, *Kern- und Elementarteilchenphysik*, VCH Verlagsgesellschaft, Weinheim (1988)

[28] W. Heitler, *The Quantum Theory of Radiation*, Clarendon Press, Oxford (1954)

[29] S.P. Møller, *Crystal Channeling or How to Build a '1000 Tesla Magnet'*, CERN-94-05 (1994)

[30] D.S. Gemmell, Channeling and Related Effects in the Motion of Charged Particles through Crystals, *Rev. Mod. Phys.* **46** (1974) 129–227

[31] K. Kleinknecht, *Detektoren für Teilchenstrahlung*, Teubner, Stuttgart (1984, 1987, 1992); *Detectors for Particle Radiation*, Cambridge University Press, Cambridge (1986)

[32] F. Sauli, *Principles of Operation of Multiwire Proportional and Drift Chambers*, CERN-77-09 (1977) and references therein

[33] N.I. Koschkin & M.G. Schirkewitsch, *Elementare Physik*, Hanser, München/Wien (1987)

[34] U. Fano, Ionization Yield of Radiations. II. The Fluctuation of the Number of Ions, *Phys. Rev.* **72** (1947) 26–9

[35] A.H. Walenta, *Review of the Physics and Technology of Charged Particle Detectors*, Preprint University of Siegen SI-83-23 (1983)

[36] G. Lutz, *Semiconductor Radiation Detectors*, Springer, Berlin (1999)

[37] H.A. Bethe, Molière's Theory of Multiple Scattering, *Phys. Rev.* **89** (1953) 1256–66

[38] C. Grupen, *Physics for Particle Detection*, Siegen University publication ed. B. Wenclawiak, S. Wilnewski (2004); Proceedings of the 10 ICFA School on Instrumentation in Elementary Particle Physics Itacuruça, Rio de Janeiro 2003 (to be published 2007); www.cbpf.br/icfa2003/

[39] H.A. Bethe & W. Heitler, Stopping of Fast Particles and Creation of Electron Pairs, *Proc. R. Soc. Lond.* **A146** (1934) 83–112

[40] E. Lohrmann, *Hochenergiephysik*, Teubner, Stuttgart (1978, 1981, 1986, 1992)

[41] U. Amaldi, Fluctuations in Calorimetric Measurements, *Phys. Scripta* **23** (1981) 409–24
[42] W. Lohmann, R. Kopp & R. Voss, *Energy Loss of Muons in the Energy Range 1 – 10.000 GeV*, CERN-85-03 (1985)
[43] M.J. Tannenbaum, *Simple Formulas for the Energy Loss of Ultrarelativistic Muons by Direct Pair Production*, Brookhaven National Laboratory, BNL-44554 (1990)
[44] W.K. Sakumoto *et al.*, Measurement of TeV Muon Energy Loss in Iron, University of Rochester UR-1209 (1991); *Phys. Rev.* **D45** (1992) 3042–50
[45] K. Mitsui, Muon Energy Loss Distribution and its Applications to the Muon Energy Determination, *Phys. Rev.* **D45** (1992) 3051–60
[46] Lev I. Dorman, *Cosmic Rays in the Earth's Atmosphere and Underground*, Kluwer Academic Publishers, Dordercht (2004)
[47] R. Baumgart *et al.*, Interaction of 200 GeV Muons in an Electromagnetic Streamer Tube Calorimeter, *Nucl. Instr. Meth.* **A258** (1987) 51–7
[48] G. Hertz, *Lehrbuch der Kernphysik*, Bd. 1, Teubner, Leipzig (1966)
[49] J.S. Marshall & A.G. Ward, Absorption Curves and Ranges for Homogeneous β-Rays, *Canad. J. Res.* **A15** (1937) 39–41
[50] E. Sauter, *Grundlagen des Strahlenschutzes*, Siemens AG, Berlin/München (1971); *Grundlagen des Strahlenschutzes*, Thiemig, München (1982)
[51] A.G. Wright, A Study of Muons Underground and Their Energy Spectrum at Sea Level, Polytechnic of North London Preprint (1974); *J. Phys.* **A7** (1974) 2085–92
[52] R.K. Bock & A. Vasilescu, *The Particle Detector Briefbook*, Springer, Heidelberg (1998)
[53] P. Marmier & E. Sheldon, *Physics of Nuclei and Particles*, Vol. 1, Academic Press, New York (1969)
[54] E. Fenyves & O. Haimann, *The Physical Principles of Nuclear Radiation Measurements*, Akadémiai Kiadó, Budapest (1969)
[55] O. Klein & Y. Nishina, Über die Streuung von Strahlung durch freie Elektronen nach der neuen relativistischen Quantenmechanik von Dirac, *Z. Phys.* **52** (1929) 853–68
[56] R.D. Evans, *The Atomic Nucleus*, McGraw-Hill, New York (1955)
[57] W.S.C. Williams, *Nuclear and Particle Physics*, Clarendon Press, Oxford (1991)
[58] V. Telnov, *Photon Collider at TESLA*, hep-ex/0010033v4 (2000); *Nucl. Instr. Meth.* **A472** (2001) 43
[59] C. Grupen & E. Hell, Lecture Notes, *Kernphysik*, University of Siegen (1983)
[60] H.A. Bethe & J. Ashkin, Passage of Radiation through Matter, in E. Segrè (ed.), *Experimental Nucl. Phys.*, Vol. 1, John Wiley & Sons Inc. (Wiley Interscience), New York (1953) 166–201
[61] G.W. Grodstein, *X-Ray Attenuation Coefficients from 10 keV to 100 MeV*, Circ. Natl. Bur. Stand. No. 583 (1957)
[62] G.R. White, *X-ray Attenuation Coefficients from 10 keV to 100 MeV*, Natl. Bur. Standards (U.S.) Rept. 1003 (1952)

2 Units of radiation measurement

Many measurements and tests with detectors are made with radioactive sources. Radiation aspects are also an issue at any accelerator and, in particular, at hadron colliders. Even at neutrino factories the radiation levels can be quite high. Basic knowledge of the units of radiation measurement and the biological effects of radiation are therefore useful [1–5].

Let us assume that there are initially N_0 nuclei of a certain radioactive element. The number will decrease in the course of time t due to decay according to

$$N = N_0 \, \mathrm{e}^{-t/\tau} \ , \tag{3.1}$$

where τ is the *lifetime* of the radioisotope. One has to distinguish between the lifetime and the *half-life* $T_{1/2}$. The half-life can be calculated from Eq. (3.1) as

$$N(t = T_{1/2}) = \frac{N_0}{2} = N_0 \, \mathrm{e}^{-T_{1/2}/\tau} \ , \tag{3.2}$$

$$T_{1/2} = \tau \cdot \ln 2 \ . \tag{3.3}$$

The decay constant of the radioactive element is

$$\lambda = \frac{1}{\tau} = \frac{\ln 2}{T_{1/2}} \ . \tag{3.4}$$

The activity of a source gives the number of decays per unit time,

$$A = -\frac{\mathrm{d}N}{\mathrm{d}t} = \frac{1}{\tau}N = \lambda N \ . \tag{3.5}$$

The unit of the activity is *Becquerel* (Bq). 1 Bq means 1 decay per second. (In passing it should be mentioned that the physical quantity with the dimension s^{-1} already has a name: Hertz! However, this unit Hz is mostly used for periodic phenomena, while Bq is used for statistically distributed events.) The unit Bq supersedes the old unit Curie (Ci). Historically 1 Ci was the activity of 1 g of radium,

$$1\,\mathrm{Ci} = 3.7 \cdot 10^{10}\,\mathrm{Bq} \tag{3.6}$$

or

$$1\,\mathrm{Bq} = 27 \cdot 10^{-12}\,\mathrm{Ci} = 27\,\mathrm{pCi} \ . \tag{3.7}$$

1 Bq is a very small unit of the activity. The radioactivity of the human body amounts to about 7500 Bq, mainly due to ^{14}C, ^{40}K and ^{232}Th.

The activity in Bq does not say very much about possible biological effects. These are related to the energy which is deposited per unit mass by a radioactive source.

The *absorbed dose* D (absorbed energy per mass unit)

$$D = \frac{1}{\varrho}\frac{\mathrm{d}W}{\mathrm{d}V} \tag{3.8}$$

($\mathrm{d}W$ – absorbed energy; ϱ – density; $\mathrm{d}V$ – unit of volume) is measured in *Grays* (1 Gray = 1 J/kg). The old cgs unit rad (**r**öntgen **a**bsorbed **d**ose, 1 rad = 100 erg/g) is related to Gray according to

$$1\,\mathrm{Gy} = 100\,\mathrm{rad} \ . \tag{3.9}$$

Gray and rad describe only the physical energy absorption, and do not take into account any biological effect. Since, however, α-, β-, γ- and neutron-emitting sources have different biological effects for the same energy absorption, a ***r**elative **b**iological **e**ffectiveness* (RBE) is defined. The absorbed dose D_γ obtained from the exposure to γ or X rays serves as reference. The absorbed dose of an arbitrary radiation which yields the same biological effect as D_γ leads to the definition of the relative biological effectiveness as

$$D_\gamma = RBE \cdot D \ . \tag{3.10}$$

The RBE factor has a complicated dependence on the radiation field, the radiation energy and the dose rate. For practical reasons, therefore,

Table 3.1. *Radiation weighting factors* w_R

Radiation and energy range	Radiation weighting factor w_R
Photons, all energies	1
Electrons and muons, all energies	1
Neutrons $E_n < 10\,\mathrm{keV}$	5
$10\,\mathrm{keV} \le E_n \le 100\,\mathrm{keV}$	10
$100\,\mathrm{keV} < E_n \le 2\,\mathrm{MeV}$	20
$2\,\mathrm{MeV} < E_n \le 20\,\mathrm{MeV}$	10
$E_n > 20\,\mathrm{MeV}$	5
Protons, except recoil protons, $E > 2\,\mathrm{MeV}$	5
α particles, nuclear fragments, heavy nuclei	20

a *radiation weighting factor* w_R (formerly called *quality factor*) is introduced. The absorbed dose D multiplied by this weighting factor is called *equivalent dose* H. The unit of the equivalent dose is 1 *Sievert* (Sv),

$$H\{\mathrm{Sv}\} = w_R \cdot D\,\{\mathrm{Gy}\} \ . \tag{3.11}$$

The weighting factor has the unit Sv/Gy. The old cgs unit rem ($H\{\mathrm{rem}\} = w_R \cdot D\{\mathrm{rad}\}$, rem = **r**öntgen **e**quivalent **m**an) is related to Sievert according to

$$1\,\mathrm{Sv} = 100\,\mathrm{rem} \ . \tag{3.12}$$

The radiation weighting factors w_R are listed in Table 3.1.

According to Table 3.1, neutrinos do not present a radiation hazard. This is certainly true for natural neutrino sources, however, the high flux of energetic neutrinos from future neutrino factories might present a radiation problem.

It should be mentioned that the biological effect of radiation is also influenced by, for example, the time sequence of absorption (e.g. fractionated irradiation), the energy spectrum of radiation, or the question whether the irradiated person has been sensitised or desensitised by a pharmaceutical drug.

The biological effect also depends on which particular part of the human body is irradiated. To take account of this effect a further *tissue weighting factor* w_T is introduced leading to a general expression for the effective equivalent dose

$$H_{\mathrm{eff}} = \sum_T w_T\, H_T \ , \tag{3.13}$$

Table 3.2. *Tissue weighting factors* w_R

Organ or tissue	Tissue weighting factor w_T
Gonads	0.20
Red bone marrow	0.12
Colon	0.12
Lung	0.12
Stomach	0.12
Bladder	0.05
Chest	0.05
Liver	0.05
Oesophagus	0.05
Thyroid gland	0.05
Skin	0.01
Bone surface	0.01
Other organs or tissue	0.05

where the sum extends over those irradiated parts of the human body which have received the doses H_T. The tissue weighting factors are listed in Table 3.2.

The most general form of the effective equivalent dose is therefore

$$H_{\text{eff}} = \sum_T w_T \sum_R w_R \, D_{T,R} \ , \tag{3.14}$$

where the sums run over the partial body doses received in different radiation fields properly weighted by the radiation and tissue weighting factors.

The *equivalent whole-body dose rate* from pointlike radiation sources can be calculated from the relation

$$\dot{H} = \Gamma \, \frac{A}{r^2} \ , \tag{3.15}$$

where A is the activity (in Bq) and r the distance from the source in metres. Γ is the dose constant which depends on the radiation field and the radioisotope. Specific γ-ray dose constants ($\Gamma_\gamma = 8.46 \cdot 10^{-14} \, \frac{\text{Sv}\cdot\text{m}^2}{\text{Bq}\cdot\text{h}}$ for ^{137}Cs) and β-ray dose constants ($\Gamma_\beta = 2.00 \cdot 10^{-11} \, \frac{\text{Sv}\cdot\text{m}^2}{\text{Bq}\cdot\text{h}}$ for ^{90}Sr) are listed in the literature [4].

Apart from these units, there is still another one describing the quantity of produced charge, which is the *Röntgen* (R). One Röntgen is the

radiation dose for X-ray or γ radiation which produces, under normal conditions, one electrostatic charge unit (esu) of electrons and ions in $1\,\mathrm{cm}^3$ of dry air.

The charge of an electron is $1.6 \cdot 10^{-19}\,\mathrm{C}$ or $4.8 \cdot 10^{-10}\,\mathrm{esu}$. (The esu is a cgs unit with $1\,\mathrm{esu} = \frac{1}{3 \cdot 10^9}\,\mathrm{C}$.) If one electrostatic charge unit is produced, the number of generated electrons per cm^3 is given by

$$N = \frac{1}{4.8 \cdot 10^{-10}} = 2.08 \cdot 10^9 \ . \tag{3.16}$$

If the unit Röntgen is transformed into an ion charge per kg, it gives

$$1\,\mathrm{R} = \frac{N \cdot q_e \ \{\mathrm{C}\}}{m_{\mathrm{air}}(1\,\mathrm{cm}^3)\ \{\mathrm{kg}\}} = \frac{1\,\mathrm{esu}}{m_{\mathrm{air}}(1\,\mathrm{cm}^3)\ \{\mathrm{kg}\}} \ , \tag{3.17}$$

where q_e is the electron charge in Coulomb, $m_{\mathrm{air}}(1\,\mathrm{cm}^3)$ is the mass of $1\,\mathrm{cm}^3$ air; consequently

$$1\,\mathrm{R} = 2.58 \cdot 10^{-4}\,\mathrm{C/\,kg} \quad \text{for air} \ . \tag{3.18}$$

If Röntgen has to be converted to an absorbed dose, one has to consider that the production of an electron–ion pair in air requires an energy of about $W = 34\,\mathrm{eV}$,

$$1\,\mathrm{R} = N \cdot \frac{W}{m_{\mathrm{air}}} = 0.88\,\mathrm{rad} = 8.8\,\mathrm{mGy} \ . \tag{3.19}$$

To obtain a feeling for these abstract units, it is quite useful to establish a natural scale by considering the radiation load from the environment.

The radioactivity of the human body amounts to about 7500 Bq, mainly caused by the radioisotope $^{14}\mathrm{C}$ and the potassium isotope $^{40}\mathrm{K}$. The average radioactive load (at sea level) by cosmic radiation ($\approx 0.3\,\mathrm{mSv/a}$)*, by terrestrial radiation ($\approx 0.5\,\mathrm{mSv/a}$) and by incorporation of radioisotopes (inhalation $\approx 1.1\,\mathrm{mSv/a}$, ingestion $\approx 0.3\,\mathrm{mSv/a}$) are all of approximately the same order of magnitude, just as the radiation load caused by civilisation ($\approx 1.0\,\mathrm{mSv/a}$), which is mainly caused by X-ray diagnostics and treatment and by exposures in nuclear medicine. The total annual per capita dose consequently is about 3 mSv.

The natural radiation load, of course, depends on the place where one lives; it has a typical fluctuation corresponding to a factor of two. The radiation load caused by civilisation naturally has a much larger fluctuation. The average value in this case results from relatively high doses obtained by few persons.

---

* a (Latin) = annum = year.

The *lethal whole-body dose* (50% mortality in 30 days without medical treatment) is 4 Sv (= 400 rem).

The International Commission for Radiological Protection (ICRP) has recommended a limit for the whole-body dose for persons working in controlled areas of 20 mSv/a (=2 rem/a) which has been adopted in most national radiation protection regulations. The ICRP has also proposed *exemption limits* for the handling of radioactive sources (e.g. 10^4 Bq for ^{137}Cs) and *clearance levels* for discharging radioactive material from radiation areas (e.g. 0.5 Bq/g for solid or liquid material containing ^{137}Cs). A radiation officer has to be installed whose responsibility is to watch that the various radiation protection regulations are respected.

References

[1] G.F. Knoll, *Radiation Detection and Measurement*, 3rd edition, John Wiley & Sons Inc., New York (Wiley Interscience), New York (1999/2000)

[2] James E. Martin, *Physics for Radiation Protection*, John Wiley & Sons Inc., New York (2000)

[3] E. Pochin, *Nuclear radiation: Risks and Benefits*, Clarendon Press, Oxford (1983)

[4] C. Grupen, *Grundkurs Strahlenschutz*, Springer, Berlin (2003)

[5] Alan Martin, Samuel A. Harbison, *An Introduction to Radiation Protection*, 3rd edition, Chapman and Hall, London (1987)

[6] Particle Data Group, Review of Particle Physics, S. Eidelman *et al.*, *Phys. Lett.* **B592 Vol. 1–4** (2004) 1–1109; W.-M. Yao *et al.*, *J. Phys.* **G33** (2006) 1–1232; http://pdg.lbl.gov

[7] Edgardo Browne & Richard B. Firestone, *Table of Radioactive Isotopes*, John Wiley & Sons Inc., New York (1986)

[8] Richard B. Firestone & Virginia S. Shirley, *Table of Isotopes*, 8th edition, Wiley Interscience, New York (1998)

[9] C. M. Lederer, *Table of Isotopes*, John Wiley & Sons Inc., New York (1978)

[10] H. Landolt & R. Börnstein, *Atomkerne und Elementarteilchen*, Vol. 5, Springer, Berlin (1952)

[11] Landolt–Börnstein, *Group I Elementary Particles, Nuclei and Atoms*, Springer, Berlin (2004), also as on-line version, see www.springeronline.com

[12] R.C. Weast & M.J. Astle (eds.), *Handbook of Chemistry and Physics*, CRC Press, Boca Raton, Florida (1979, 1987)

[13] C. Grupen, *Astroparticle Physics*, Springer, New York (2005)

3 Practical Radiation Dosimetry at Accelerators

An online version of the book is published at https://doi.org/10.1007/978-3-030-57031-6 .

The radiation fields around a working particle accelerator are consisting of different types of ionising radiation, extending over broad ranges of energies. This makes dose equivalent measurements at accelerators challenging, and special instruments have been developed over the years to cope with the characteristics of these fields. In shutdown periods, when the accelerator is stopped, the origin of radiation is activated material, containing relatively long-lived radioactive nuclei (with half-lives of days to years), created in beam-matter interactions during the preceding operation periods of the accelerator. These nuclei emit gamma (photon) and beta (electron/positron) radiation. Dose equivalent of these radiations can be measured with standard radiation protection dosimeters and survey instruments, as developed for dosimetry in nuclear and medical radiation facilities.

In a radiation protection program at an accelerator facility, radiation measurement is essential for the following tasks

- measuring dose equivalent at workplaces to make a prospective assessment of working conditions, and to demonstrate the adequacy of the radiation shielding put in place;
- monitoring the dose equivalent to personnel, to demonstrate compliance with legal dose limits;
- monitoring radiation emitted to the environment, to demonstrate compliance with emission and immission limits (Sect. 4.6.1).

Dosimeters are used to measure dose or dose equivalent. In this section, the term *dosimeter* is used likewise for passive and active devices whose purpose is the measurement of dose equivalent. Based on their area of usage, they are may be *personal dosimeters*, *radiation survey instrument* or *radiation monitors*.

One distinguishes between passive and active dosimeters.

- Passive dosimeters are based on a physical effect which is (roughly) proportional to dose equivalent. The magnitude of the physical effect creates a proportional signal once they are read-out after a defined period of exposure. They are used when the immediate display of a result is not essential, for example for personal

dosimetry at workplaces with a moderate dose equivalent rate, or for long-term monitoring of the environment.

- Active dosimeters have a detection mechanism which can be directly converted to an electrical signal. Active dosimeters have the advantage to give an immediate display of the dose equivalent, but they are usually larger and more expensive than passive dosimeters. They are used in the form of *electronic personal dosimeters* to monitor workers at workplaces where the dose equivalent rate is so high that they could accumulate a significant fraction of the dose limit in a short time. Active dosimeters are also used for radiation surveys, and as alarm monitors where sudden increases of the radiation intensity are possible and Survey instruments and active radiation monitors usually indicate the instantaneous *dose equivalent rate* $\dot{H} = {}^{dH}\!/_{dt}$.

Many detectors based on different physical principles exist for the quantification of ionising radiation. Only few of them can be employed as a radiation dosimeter. To make a good dosimeter, the energy-dependent response of the detector to a physical quantity describing the radiation field (for example, particle fluence) must be approximately proportional to the energy dependence of the operational quantity to be measured, for example $H^*(10)$. Hardly any physical radiation detector shows spontaneously the required proportionality of the physical effect to dose equivalent to be used as a radiation dosimeter. It is necessary to modify the energy response of the physical detector to mimic the energy dependence of the dose equivalent quantity to be measured.

This section can only give a very short overview about radiation detection and dosimetry. [20] or [19] give a more detailed treatment of radiation detection, whereas [22] is still a standard reference for radiation dosimetry. [12] gives a modern account of this subject.

3.4.2.1 Photon (Gamma) Dosimeters

The largest fraction of dose equivalent to which workers are exposed in accelerator facilities comes from photons and is accumulated during shutdown periods when the accelerators are maintained. The source of the photons is material activated by interactions with particles during the preceding operational periods. The isotope content of activation products in accelerator facilities is different from those in the nuclear industry by type and concentration, but the same methods of detection and measurement can be employed. Long-lived activation products emit gamma (photon) and beta (electron or positron) radiation.

Photons are indirectly ionising particles, as a first step to detection a secondary electron must be created by the photoelectric effect or by Compton scattering. Most active photon dosimeters rely on one of two detection mechanisms: gas ionisation and creation of free charges in semiconductors. Passive photon dosimeters use thermoluminescence (TL) and optically stimulated luminescence (OSL) as detection principles. Photographic film has been replaced by these technologies in most applications.

Three different types of gas-filled detectors for photons are used in radiation protection: ionisation chambers, proportional counters, and Geiger-Müller counters. The commercially available types have in common a cylindrical geometry with a collection anode in the centre (in proportional counters and GM counters, an anode wire) (Fig. 3.5). Secondary electrons are created in the detector wall and registered in the filling gas by ionisation. The average energy to create an electron-ion pair in gases, the ionisation energy, lies between 20 eV and 40 eV, for air it is approximately 32 eV. The charges are separated by an electrical field between the anode and the chamber wall, and electrons drift to the central anode. The chamber constitutes a cylindrical capacitor for which the radial component peaks at the anode wire.

The three types of gaseous detectors can be distinguished by applied voltage V_0 between chamber wall (cathode) and central anode:

- Ionisation chambers for radiation protection operate usually in DC mode, with a low-pass filter connected to the anode. The applied voltage V_0 is in the leftmost region in Fig. 3.6, high enough to separate the created electron-ion pairs before they can recombine. The ionisation current comes from the electron-ion pairs created by the secondary electron along its path and is proportional to the energy deposited in the gas by the incident radiation.
- In proportional counters, the field strength *E(r)* close to the wire is high enough to ionise additional atoms by the secondary electrons. A charge avalanche with an amplification factor $A \approx 10^2 \cdots 10^6$ will result. In a certain voltage range, depending on the gas type and pressure and chamber geometry, the amplification factor A is independent of the energy of the incoming particle, and the thus signal amplitude proportional to particle energy. This is the proportional regime.
- In a Geiger-Müller counter, the electrical field close to the anode wire is so high that the charge avalanche triggers further avalanches all along the wire and depletes the counting gas from neutral atoms. In this regime, the amplification factor is $A \approx 10^{10}$ and independent from the energy of the incoming particle.

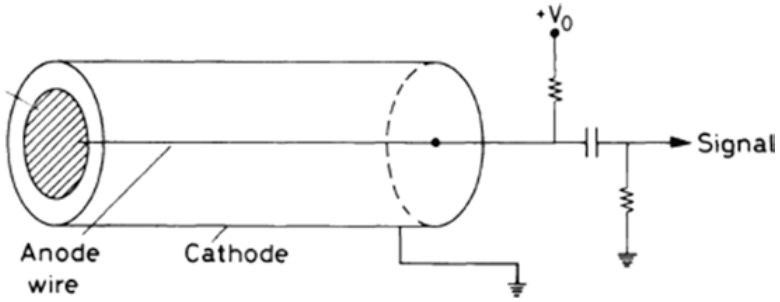

Fig. 3.5 Schematic construction of a gas-filled detector for ionising radiation. (Adapted from [20]. Here, the signal is coupled out with a high-pass filter, in DC ionisation chambers, a low-pass filter would be employed, by changing the position of capacity and resistor to ground)

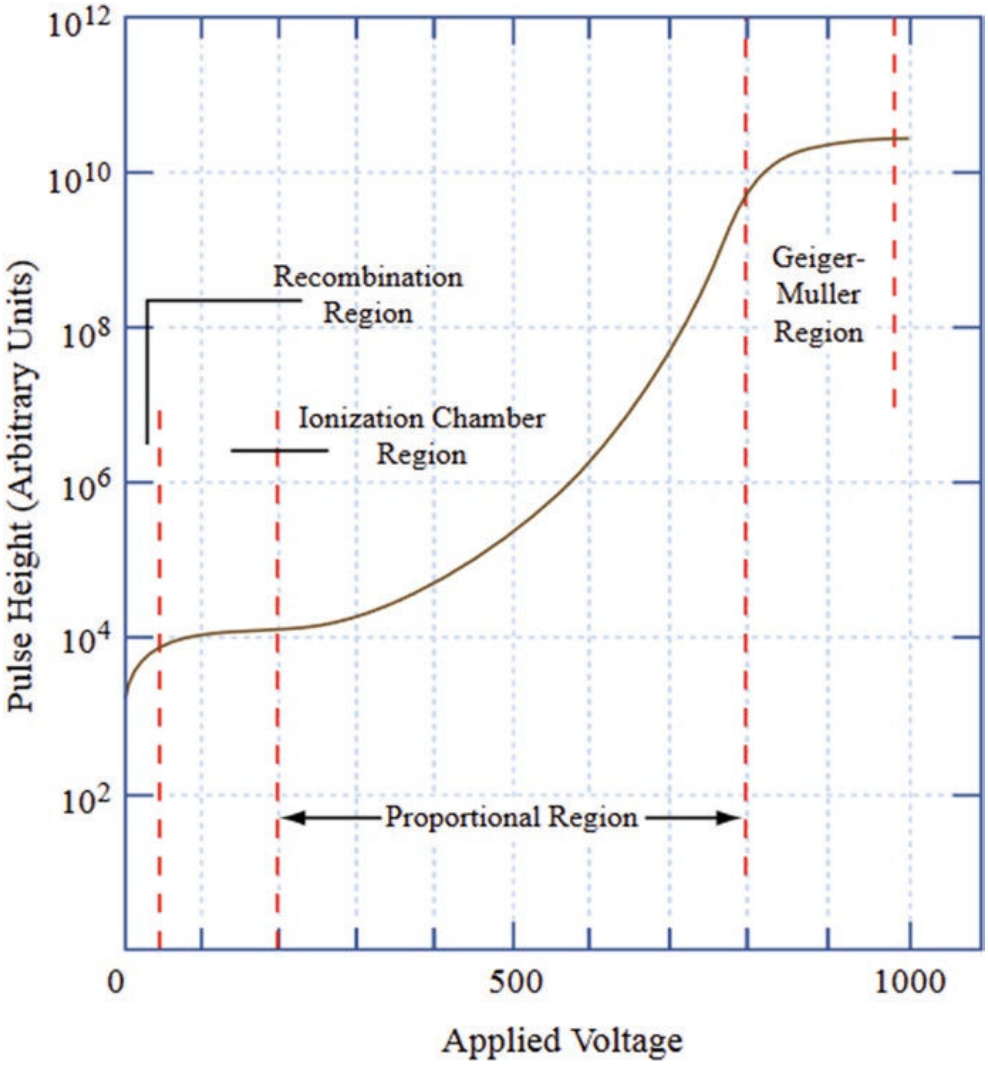

Fig. 3.6 Signal height collected versus applied voltage in gas-filled radiation detectors with central wire. (After [20])

The energy dependence of the three gaseous detector types is mainly determined by the probability that a photon interacts in the wall and emits secondary electrons into the counting gas. Ionisation chambers with walls made from tissue equivalent (TE) plastic and filled with TE gas give a signal proportional to absorbed dose in tissue, which is a good approximation of dose equivalent for photons and electrons. For other particles, a so-called *quality factor* must be applied. In instruments based on Geiger-Müller and proportional counters, metallic filters are placed around the counter chamber to influence the energy dependence of their response to photons. This strategy is successful in a limited energy range, usually between 50 keV and 1.3 MeV or 3 MeV. Below this interval, the dosimeters are insensitive (low energy photons are absorbed ion the detector wall), above they have a strong overresponse.

Proportional counters and Geiger-Müller counters are light and small, their sensitivity is ideally suited to assess photon radiation from activated accelerator components. Ionisation chambers can be used to monitor the radiation emitted by an accelerator in operation. For this, their factory calibration to reference photon sources, must be adapted to take account of the mixed radiation field.

References

Safety Process

1. L.A. Cox, What's wrong with risk matrices ? Risk Analysis **28**(2) (2008)
2. Deutsche Gesetzliche Unfallversicherung – Spitzenverband. Prävention https://www.dguv.de/de/praevention/index.jsp
3. Health and Safety Executive (United Kingdom), *Risk Management- Frequently Asked Questions – What are risk matrices?* http://www.hse.gov.uk/risk/faq.htm#q27
4. Health and Safety Executive, ICMESA chemical company, Seveso, Italy. 10th July 1976, http://www.hse.gov.uk/comah/sragtech/caseseveso76.htm
5. Health and Safety Executive, Guidance, http://www.hse.gov.uk/guidance/index.htm
6. Institut national de recherche. et de sécurité, Démarches de prevention, http://www.inrs.fr/demarche/
7. S. Mannan (ed.) Lees' Loss Prevention in the Process Industries (Fourth Edition), Chapter 9 (Butterworth-Heinemann 2012)
8. MYRRHA, Multi-purpose hYbrid Research Reactor for High-tech Applications. https://www.myrrha.be/
9. National Institute for Occupational Safety and Health (NIOSH), Hierarchy of Controls, https://www.cdc.gov/niosh/topics/hierarchy/#
10. B. Neeradael, The MYRRHA Project – Safety methodology and challenges, Plenary contribution at EUROSAFE Forum 2012, https://www.eurosafe-forum.org/eurosafe2012#Plenary
11. SUVA, Connaissez-vous le portefeuille des phénomènes dangereux dans votre entreprise (Luzern 2011), https://www.suva.ch/fr-CH/materiel/documentation/connaissezvous-le-potentiel-des-phenomenes-dangereux-dans-votre-entreprise%2D%2Dle%2D%2D66105-f-25527-25526

Safety Organisation

12. Health and Safety Executive, Isolation and permits to work, https://www.hse.gov.uk/safemaintenance/permits.htm
13. Health and Safety Executive, Human factors: Permit to work systems, https://www.hse.gov.uk/humanfactors/topics/ptw.htm
14. International Labour Organization, C155 – Occupational Safety and Health Convention (Geneva 1981), https://www.ilo.org/global/standards/subjects-covered-by-international-labour-standards/occupational-safety-and-health
15. International Labour Organization, Guidelines on occupational safety and health management systems, ILO-OSH 2001, 2nd ed. (Geneva 2009) https://www.ilo.org/safework/info/standards-and-instruments/WCMS_107727

Beam Safety

16. R. Schmidt, in Proceedings of the Joint International Accelerator School: Beam Loss and Accelerator Protection, Newport Beach, United States, 5–14 November 2014, edited by R. Schmidt, CERN-2016-002 (CERN, Geneva, 2016), pp. 1–20, doi:10.5170/CERN-2016-002.1
17. R. Schmidt, in *Proceedings of the Joint International Accelerator School: Beam Loss and Accelerator Protection*, Newport Beach, United States, 5–14 November 2014, edited by R. Schmidt, CERN-2016-002 (CERN, Geneva, 2016), pp. 319–341, https://doi.org/10.5170/CERN-2016-002.319

18. E. Carrone, in Proceedings of the Joint International Accelerator School: Beam Loss and Accelerator Protection, Newport Beach, United States, 5–14 November 2014, edited by R. Schmidt, CERN-2016-002 (CERN, Geneva, 2016), pp. 271–302 doi:10.5170/CERN-2016-002.271
19. Health and Safety Executive, Functional safety, https://www.hse.gov.uk/eci/functional.htm
20. International Electrotechnical Commission, Functional safety of electrical/electronic/programmable electronic safety-related systems, Part 0: Functional safety and IEC 61508; IEC 61508-0 (Geneva 2005)
21. International Electrotechnical Commission, Safety of machinery – Functional safety of safety-related electrical, electronic, and programmable electronic control systems, IEC 62061 (Geneva 2005)
22. International Electrotechnical Commission, Functional safety of electrical/electronic/programmable electronic safety-related systems, Part 1 – 7; IEC 61508-1 to IEC 61508-7 (Geneva 2010)
23. International Electrotechnical Commission, Functional safety – Safety instrumented systems for the process industry, Part 1-3, IEC 61511 Part 1 to 3 (Geneva 2016)
24. VDE Prüf- und Zertifizierungsinstitut, Funktionale Sicherheit – Prüfung und Zertifizierung im VDE-Institut, https://www.vde.com/tic-de/dienstleistungen/funktionale-sicherheit

4 Experimental setup- and procedures

4.1 Operation principle of the AREAL photoinjector

The experiment will be conducted at the AREAL photoinjector, as depicted schematically in Fig.1. In summary, the operational principle of the photoinjector can be outlined as follows:

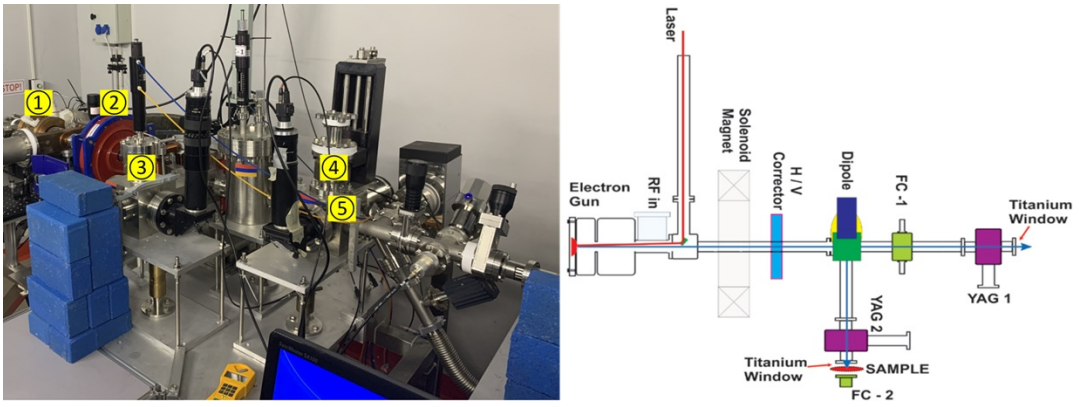

Figure 1: Photo (left) and schematic (right) of the AREAL photoinjector. In the right the RF-gun ①, solenoid ②, YAG-2 ③, YAG-1 ④ as well as the Farday-cup ⑤ are shown.

a) A specialized mirror beamline is employed to redirect a ps-short UV laser pulse toward the Cu-photocathode, which is positioned within a vacuum at the rear of the RF cavity (Fig.1 ①). The photon energy exceeds the work function of the metal, resulting in the ejection of photoelectrons from the cathode surface. The extracted charge varies with operation parameters. The typical range of this variation is from a few tens to a few hundreds of pC.

b) Subsequently, the emitted photoelectrons are accelerated by the electric field within the RF cavity. The high field gradient of ~ 10 MV/m results in the particles attaining relativistic velocity upon exiting the RF gun, with a typical energy that is on the order of several MeV. The electron beam is characterized by a pulsed structure, a feature that is analogous to the pulsed operation of the photoinjector laser. The beam is composed of individual particle packets, which are referred to as bunches.

c) In the downstream region of the RF gun, the electrons are focused by the solenoid (Fig.1 ②) and quadrupoles. The beam is steered towards a variety of diagnostic instruments, including YAG screens (③, ④) and Faraday cup (⑤), using dipole magnets.

The process discussed in items a)-c) above is repeated at a *repetition rate* **n** that can be set between 1 and 20 Hz.

4.2 Principle of Faraday cup charge measurement

Beam charge measurement using a Faraday cup is invasive (see Fig.2) i.e. the cup is inserted directly into the path of the beam, which is completely absorbed by the conducting material of the cup. The voltage

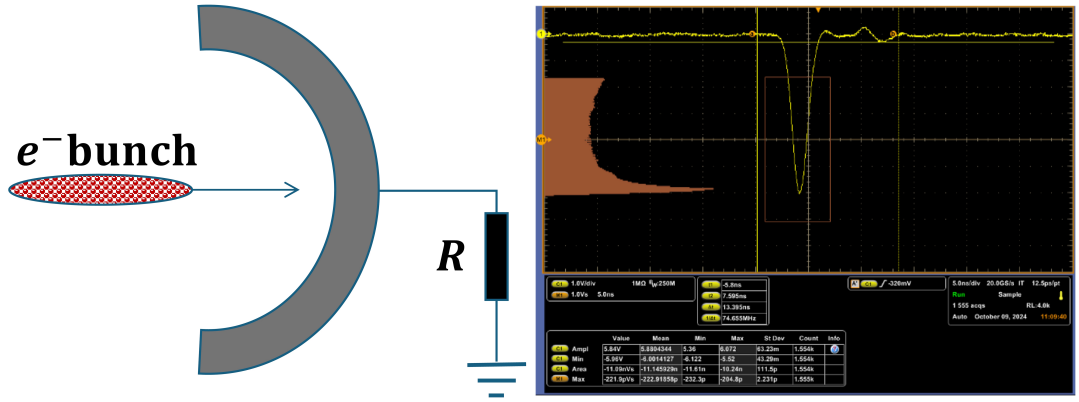

Figure 2: Schematic of the Faraday cup bunch charge measurement (left) and scope trace of the measurement (right).

$V(t)$ measured across a resistor R to ground provides a measure of the instantaneous current absorbed. Ideally, the goal is to find the integral:

$$Q_{bunch} = \frac{1}{R}\int_{-\infty}^{\infty} V(t)dt \tag{1}$$

in order to obtain the total bunch charge Q_{bunch}. In practice, the oscilloscope installed in the AREAL-control room integrates the voltage signal $V(t)$ numerically and displays the result in units of $[V \cdot s]$ on the screen. Then the result has to be divided by the value of R for to obtain the charge. The time window for measurement, that is to say, the integral limits specified in Eq.1, should be adjusted in advance in the oscilloscope settings panel. An illustration of this measurement is presented in Fig.2 on the right.

4.3 Available radiation detectors

The experiment will utilize two distinct gas-filled detectors, the operation principle of which is described on page 54. The GAMMA-SCOUT (see Fig.3a) is a Geiger-Mueller-type detector that can measure radiation dose and dose rate with high precision over a wide dynamic range. An important feature is the

(a) GAMMA-SCOUT, a Geiger-Mueller radiation detector.

(b) The high-precision electrometer DOSE-1 (left) and the ionization chamber NACP-02 (right).

Figure 3: Radiation detection instumentation used in the experiment.

logging function, which allows for continuous measurement and storage of data in the onboard memory.

There is also the option to transfer the data to a connected PC. For more details, please refer to the user manual (https://www.gamma-scout.com/manual/) and the supervisor's instructions during the experiment.
When used with the NACP-02 ionization chamber as a radiation sensor (see Fig.3b), the DOSE-1 electrometer can measure dose, dose rate, and adsorbed charge. Adsorbed charge measurements serve as an alternative to the Faraday cup method described above. An overview of the DOSE-1 features is available online (http://www.teramed.com.tr/wp-content/uploads/2016/04/RT-BR-E-DOSE1_Rev.1_0211_0.pdf), and the supervisor will provide more details during the practical course.

4.4 Experimental tasks

4.4.1 Radiation protection and practical dosimetry at AREAL

This experiment aims to monitor radiation doses and rates at two locations: the AREAL tunnel (T) and the control room (C). Two GAMMA SCOUT detectors have been installed at these locations. The dosimeters operate in logging mode, measuring and storing data every 30 minutes. Since the measurements are automatic, no manual intervention is necessary and the dosimeters can be left unattended for one to two days. A large amount of data should be collected during this time. It is essential that AREAL operates with a beam sufficiently long during the measurement period. Once the measurement is finished, connect to a PC and export the data for analysis. First split the data into four sets as follows:

- data set C_{OFF} - in the control room, when AREAL-beam was OFF.
- data set C_{ON} - in the control room, when AREAL-beam was ON.
- data set T_{OFF} - in the tunnel, when AREAL-beam was OFF.
- data set T_{ON} - in the tunnel, when AREAL-beam was ON.

Answer these questions:

- What are the mean values of C_{OFF} and C_{ON}? Compare them with the natural radiation dose rate in the Yerevan area.
- Are C_{ON} and T_{ON} correlated?
- Statistically speaking, are the two samples C_{OFF} and C_{ON} drawn from the same parent distribution? *Hint:* Consider using the *ks_2samp()* function from the *scipy.stats* Python package. The underlying theory is explained on page 341 of the textbook *Introduction to Statistics and Data Analysis for Physicists* by Gerhard Bohm and Günter Zech, which can be downloaded from the DESY library: https://bib-pubdb1.desy.de/record/389738/files/vstatmp_e17.pdf

4.4.2 Investigations of the absorbed dose rate of irradiated samples

The objective of this experiment is to determine the absorbed dose rate of a sample mounted at the end of the AREAL electron beamline. This sample is directly irradiated by the electron beam. The dose rate $\dot{D}$ will be first calculated analytically using the relation:

$$\dot{D} = \frac{Q_{bunch} \cdot n}{e \cdot A} \cdot \left(\frac{S}{\rho}\right)_{col} \tag{2}$$

where A is the beam crosssection at the sample location, and $\left(\frac{S}{\rho}\right)$ is the mass stopping power, which depends on the electron energy, e is the elementary charge and n the beam repetition rate. The analytical dose rate estimation provided by the above equation requires the following intermediate steps:

i The electron beam's charge Q_{bunch} and energy E_{beam} must be measured using standard beam diagnostics. This task may be completed with another group working on a similar task, such as the experiments "Electron Beam Parameter Measurements" and/or "Generation of Ultrashort Relativistic Electron Beams."

ii Find the value of the mass stopping power $\left(\frac{S}{\rho}\right)$ corresponding to E_{beam}. This can easily be found on the website of the United States' National Institute of Standards and Technology (NIST): `https://physics.nist.gov/PhysRefData/Star/Text/ESTAR.html`

iii The beam crossection A must be measured as well. There are two options for that. The first one is to measure the beam size using the screen $YAG-1$ (see Fig.1) and *assume* that it is the same at the very end of the beamline, where the dose rate measurement takes place. The first option has an obvious drawback, which can be eliminated by having students manually mount a glass plate at the end of the beamline and expose it to the electron beam. The plate darkens at the points where it interacts with the electrons, and the degree of darkening is proportional to the intensity of the beam. To avoid overexposure, remove the plate after about 100 seconds of irradiation. Then, it can be scanned to obtain an electronic image that can be analyzed using software such as *ImageJ* `https://imagej.net/ij/` or a selfmade Python script.

In addition to the analytical estimate with Eq.2, the dose rate will be measured directly using the intrumentation shown in Fig.3b. For this the ionisation chamber will me mounted at the beamline end and dose rate $\dot{D}$ measured using the electrometer DOSE-1. Finally the results have to be compared and the possible error sources discussed.